Available online at www.sciencedirect.com
SCIENCE DIRECT®
Annals of Physics 315 (2005) 2–51
ANNALS of PHYSICS
www.elsevier.com/locate/aop

Supersymmetry and cosmology

Jonathan L. Feng*

Department of Physics and Astronomy, University of California, Irvine, CA 92697, USA

Received 23 February 2004; accepted 29 September 2004
Available online 19 December 2004

Abstract

Cosmology now provides unambiguous, quantitative evidence for new particle physics. I discuss the implications of cosmology for supersymmetry and vice versa. Topics include: motivations for supersymmetry; supersymmetry breaking; dark energy; freeze out and WIMPs; neutralino dark matter; cosmologically preferred regions of minimal supergravity; direct and indirect detection of neutralinos; the DAMA and HEAT signals; inflation and reheating; gravitino dark matter; Big Bang nucleosynthesis; and the cosmic microwave background. I conclude with speculations about the prospects for a microscopic description of the dark universe, stressing the necessity of diverse experiments on both sides of the particle physics/cosmology interface.

1. Introduction

Not long ago, particle physicists could often be heard bemoaning the lack of unambiguous, quantitative evidence for physics beyond their standard model. Those days are gone. Although the standard model of particle physics remains one of the great triumphs of modern science, it now appears that it fails at even the most basic level—providing a reasonably complete catalog of the building blocks of our universe.

* Corresponding author. Fax: +1 9498242174.
E-mail address: jlf@uci.edu.

0003-4916/$ - see front matter
doi:10.1016/j.aop.2004.09.014

Recent cosmological measurements have pinned down the amount of baryon, matter, and dark energy in the universe [1,2]. In units of the critical density, these energy densities are

$$\Omega_{\rm B} = 0.044 \pm 0.004, \tag{1}$$

$$\Omega_{\rm matter} = 0.27 \pm 0.04, \tag{2}$$

$$\Omega_{\Lambda} = 0.73 \pm 0.04, \tag{3}$$

implying a non-baryonic dark matter component with

$$0.094 < \Omega_{\rm DM} h^2 < 0.129 \ (95\% \ {\rm CL}), \tag{4}$$

where $h \simeq 0.71$ is the normalized Hubble expansion rate. Both the central values and uncertainties were nearly unthinkable even just a few years ago. These measurements are clear and surprisingly precise evidence that the known particles make up only a small fraction of the total energy density of the universe. Cosmology now provides overwhelming evidence for new particle physics.

At the same time, the microscopic properties of dark matter and dark energy are remarkably unconstrained by cosmological and astrophysical observations. Theoretical insights from particle physics are therefore required, both to suggest candidates for dark matter and dark energy and to identify experiments and observations that may confirm or exclude these speculations.

Weak-scale supersymmetry is at present the most well-motivated framework for new particle physics. Its particle physics motivations are numerous and are reviewed in Section 2. More than that, it naturally provides dark matter candidates with approximately the right relic density. This fact provides a strong, fundamental, and completely independent motivation for supersymmetric theories. For these reasons, the implications of supersymmetry for cosmology, and vice versa, merit serious consideration.

Many topics lie at the interface of particle physics and cosmology, and supersymmetry has something to say about nearly every one of them. Regrettably, spacetime constraints preclude detailed discussion of many of these topics. Although the discussion below will touch on a variety of subjects, it will focus on dark matter, where the connections between supersymmetry and cosmology are concrete and rich, the above-mentioned quantitative evidence is especially tantalizing, and the role of experiments is clear and promising.

Weak-scale supersymmetry is briefly reviewed in Section 2 with a focus on aspects most relevant to astrophysics and cosmology. In Sections 3 and 4 the possible roles of neutralinos and gravitinos in the early universe are described. As will be seen, their cosmological and astrophysical implications are very different; together they illustrate the wealth of possibilities in supersymmetric cosmology. I conclude in Section 5 with speculations about the future prospects for a microscopic understanding of the dark universe.

2. Supersymmetry essentials

2.1. A new spacetime symmetry

Supersymmetry is an extension of the known spacetime symmetries [3]. The spacetime symmetries of rotations, boosts, and translations are generated by angular momentum operators L_i, boost operators K_i, and momentum operators P_μ, respectively. The L and K generators form Lorentz symmetry, and all 10 generators together form Poincare symmetry. Supersymmetry is the symmetry that results when these 10 generators are further supplemented by fermionic operators Q_α. It emerges naturally in string theory and, in a sense that may be made precise [4], is the maximal possible extension of Poincare symmetry.

If a symmetry exists in nature, acting on a physical state with any generator of the symmetry gives another physical state. For example, acting on an electron with a momentum operator produces another physical state, namely, an electron translated in space or time. Spacetime symmetries leave the quantum numbers of the state invariant—in this example, the initial and final states have the same mass, electric charge, etc.

In an exactly supersymmetric world, then, acting on any physical state with the supersymmetry generator Q_α produces another physical state. As with the other spacetime generators, Q_α does not change the mass, electric charge, and other quantum numbers of the physical state. In contrast to the Poincare generators, however, a supersymmetric transformation changes bosons to fermions and vice versa. The basic prediction of supersymmetry is, then, that for every known particle there is another particle, its superpartner, with spin differing by 1/2.

One may show that no particle of the standard model is the superpartner of another. Supersymmetry therefore predicts a plethora of superpartners, none of which has been discovered. Mass degenerate superpartners cannot exist—they would have been discovered long ago—and so supersymmetry cannot be an exact symmetry. The only viable supersymmetric theories are therefore those with non-degenerate superpartners. This may be achieved by introducing supersymmetry-breaking contributions to superpartner masses to lift them beyond current search limits. At first sight, this would appear to be a drastic step that considerably detracts from the appeal of supersymmetry. It turns out, however, that the main virtues of supersymmetry are preserved even if such mass terms are introduced. In addition, the possibility of supersymmetric dark matter emerges naturally and beautifully in theories with broken supersymmetry.

2.2. Supersymmetry and the weak scale

Once supersymmetry is broken, the mass scale for superpartners is unconstrained. There is, however, a strong motivation for this scale to be the weak scale: the gauge hierarchy problem. In the standard model of particle physics, the classical mass of the Higgs boson $(m_h^2)_0$ receives quantum corrections (see Fig. 1). Including quantum corrections from standard model fermions f_L and f_R, one finds that the physical Higgs boson mass is

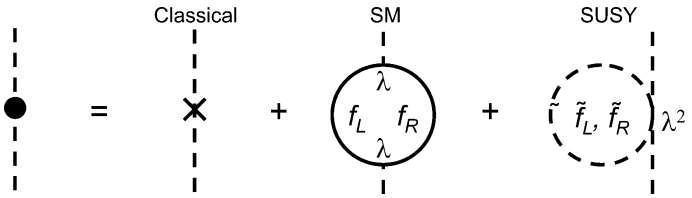

Fig. 1. Contributions to the Higgs boson mass in the standard model and in supersymmetry.

$$m_h^2 = (m_h^2)_0 - \frac{1}{16\pi^2}\lambda^2\Lambda^2 + \cdots, \tag{5}$$

where the last term is the leading quantum correction, with λ the Higgs-fermion coupling. Λ is the ultraviolet cutoff of the loop integral, presumably some high scale well above the weak scale. If Λ is of the order of the Planck scale $\sim 10^{19}$ GeV, the classical Higgs mass and its quantum correction must cancel to an unbelievable 1 part in 10^{34} to produce the required weak-scale m_h. This unnatural fine-tuning is the gauge hierarchy problem.

In the supersymmetric standard model, however, for every quantum correction with standard model fermions f_L and f_R in the loop, there are corresponding quantum corrections with superpartners $\tilde{f}_{\mathrm{L}}$ and $\tilde{f}_{\mathrm{R}}$. The physical Higgs mass then becomes

$$\begin{aligned} m_h^2 &= (m_h^2)_0 - \frac{1}{16\pi^2}\lambda^2\Lambda^2 + \frac{1}{16\pi^2}\lambda^2\Lambda^2 + \cdots \\ &\approx (m_h^2)_0 + \frac{1}{16\pi^2}(m_{\tilde{f}}^2 - m_f^2)\ln(\Lambda/m_{\tilde{f}}), \end{aligned} \tag{6}$$

where the terms quadratic in Λ cancel, leaving a term logarithmic in Λ as the leading contribution. In this case, the quantum corrections are reasonable even for very large Λ, and no fine-tuning is required.

In the case of exact supersymmetry, where $m_{\tilde{f}} = m_f$, even the logarithmically divergent term vanishes. In fact, quantum corrections to masses vanish to all orders in perturbation theory, an example of powerful non-renormalization theorems in supersymmetry. From Eq. (6), however, we see that exact mass degeneracy is not required to solve the gauge hierarchy problem. What *is* required is that the dimensionless couplings λ of standard model particles and their superpartners are identical, and that the superpartner masses be not too far above the weak scale (or else even the logarithmically divergent term would be large compared to the weak scale, requiring another fine-tuned cancellation). This can be achieved simply by adding supersymmetry-breaking weak-scale masses for superpartners. In fact, other terms, such as some cubic scalar couplings, may also be added without re-introducing the fine-tuning. All such terms are called "soft," and the theory with weak-scale soft supersymmetry-breaking terms is "weak-scale supersymmetry."

2.3. The neutral supersymmetric spectrum

Supersymmetric particles that are electrically neutral, and so promising dark matter candidates, are shown with their standard model partners in Fig. 2. In supersym-

Spin	U(1) M_1	SU(2) M_2	Down-type μ	Up-type μ	$m_{\tilde{\nu}}$	$m_{3/2}$
2						G graviton
3/2						$\tilde{G}$ gravitino
1	B	W^0				
1/2	$\tilde{B}$ Bino	$\tilde{W}^0$ Wino	$\tilde{H}_d$ Higgsino	$\tilde{H}_u$ Higgsino	ν	
0			H_d	H_u	$\tilde{\nu}$ sneutrino	

Fig. 2. Neutral particles in the supersymmetric spectrum. M_1, M_2, μ, $m_{\tilde{\nu}}$, and $m_{3/2}$ are unknown weak-scale mass parameters. The Bino, Wino, and down- and up-type Higgsinos mix to form neutralinos.

metric models, two Higgs doublets are required to give mass to all fermions. The two neutral Higgs bosons are $H_{\rm d}$ and $H_{\rm u}$, which give mass to the down-type and up-type fermions, respectively, and each of these has a superpartner. Aside from this subtlety, the superpartner spectrum is exactly as one would expect. It consists of spin 0 sneutrinos, one for each neutrino, the spin 3/2 gravitino, and the spin 1/2 Bino, neutral Wino, and down- and up-type Higgsinos. These states have masses determined (in part) by the corresponding mass parameters listed in the top row of Fig. 2. These parameters are unknown, but are presumably of the order of the weak scale, given the motivations described above.

The gravitino is a mass eigenstate with mass $m_{3/2}$. The sneutrinos are also mass eigenstates, assuming flavor and R-parity conservation (see Section 2.4). The spin 1/2 states are differentiated only by their electroweak quantum numbers. After electroweak symmetry breaking, these gauge eigenstates therefore mix to form mass eigenstates. In the basis $(-i\tilde{B}, -i\tilde{W}^3, \tilde{H}_{\rm d}, \tilde{H}_{\rm u})$ the mixing matrix is

$$\boldsymbol{M}_\chi = \begin{pmatrix} M_1 & 0 & -M_Z\cos\beta s_W & M_Z\sin\beta s_W \\ 0 & M_2 & M_Z\cos\beta c_W & -M_Z\sin\beta c_W \\ -M_Z\cos\beta s_W & M_Z\cos\beta c_W & 0 & -\mu \\ M_Z\sin\beta s_W & -M_Z\sin\beta c_W & -\mu & 0 \end{pmatrix}, \tag{7}$$

where $c_W \equiv \cos\theta_W$, $s_W \equiv \sin\theta_W$, and β is another unknown parameter defined by $\tan\beta \equiv \langle H_{\rm u}\rangle/\langle H_{\rm d}\rangle$, the ratio of the up-type to down-type Higgs scalar vacuum expectation values (vevs). The mass eigenstates are called neutralinos and denoted $\{\chi \equiv \chi_1, \chi_2, \chi_3, \chi_4\}$, in order of increasing mass. If $M_1 \ll M_2, |\mu|$, the lightest neutralino χ has a mass of approximately M_1 and is nearly a pure Bino. However, for $M_1 \sim M_2 \sim |\mu|$, χ is a mixture with significant components of each gauge eigenstate.

Finally, note that neutralinos are Majorana fermions; they are their own anti-particles. This fact has important consequences for neutralino dark matter, as will be discussed below.

2.4. R-Parity

Weak-scale superpartners solve the gauge hierarchy problem through their virtual effects. However, without additional structure, they also mediate baryon and lepton number violation at unacceptable levels. For example, proton decay $p \to \pi^0 e^+$ may be mediated by a squark as shown in Fig. 3.

An elegant way to forbid this decay is to impose the conservation of R-parity $R_p \equiv (-1)^{3(B-L)+2S}$, where B, L, and S are baryon number, lepton number, and spin, respectively. All standard model particles have $R_p = 1$, and all superpartners have $R_p = -1$. R-parity conservation implies $\Pi R_p = 1$ at each vertex, and so both vertices in Fig. 3 are forbidden. Proton decay may be eliminated without R-parity conservation, for example, by forbidding B or L violation, but not both. However, in these cases, the non-vanishing R-parity violating couplings are typically subject to stringent constraints from other processes, requiring some alternative explanation.

An immediate consequence of R-parity conservation is that the lightest supersymmetric particle (LSP) cannot decay to standard model particles and is therefore stable. Particle physics constraints therefore naturally suggest a symmetry that provides a new stable particle that may contribute significantly to the present energy density of the universe.

2.5. Supersymmetry breaking and dark energy

Given R-parity conservation, the identity of the LSP has great cosmological importance. The gauge hierarchy problem is no help in identifying the LSP, as it may be solved with any superpartner masses, provided they are all of the order of the weak scale. What is required is an understanding of supersymmetry breaking, which governs the soft supersymmetry-breaking terms and the superpartner spectrum.

The topic of supersymmetry breaking is technical and large. However, the most popular models have "hidden sector" supersymmetry breaking, and their essential features may be understood by analogy to electroweak symmetry breaking in the standard model.

The interactions of the standard model may be divided into three sectors (see Fig. 4). The electroweak symmetry breaking (EWSB) sector contains interactions involving only the Higgs boson (the Higgs potential); the observable sector contains interactions involving only what we might call the "observable fields," such

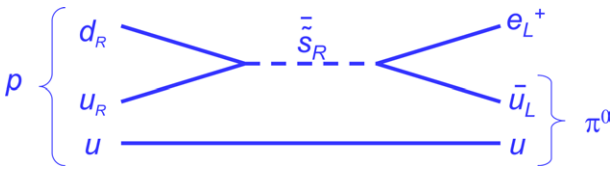

Fig. 3. Proton decay mediated by squark.

SM	EWSB Sector $h \to v$	Mediation Sector h, q, l	Observable Sector q, l
SUSY	SUSY Breaking Sector $Z \to F$	Mediation Sector Z, Q, L	Observable Sector Q, L

Fig. 4. Sectors of interactions for electroweak symmetry breaking in the standard model and supersymmetry breaking in hidden sector supersymmetry breaking models.

as quarks q and leptons l; and the mediation sector contains all remaining interactions, which couple the Higgs and observable fields (the Yukawa interactions). Electroweak symmetry is broken in the EWSB sector when the Higgs boson obtains a non-zero vev: $h \to v$. This is transmitted to the observable sector by the mediating interactions. The EWSB sector determines the overall scale of EWSB, but the interactions of the mediating sector determine the detailed spectrum of the observed particles, as well as much of their phenomenology.

Models with hidden sector supersymmetry breaking have a similar structure. They have a supersymmetry breaking sector, which contains interactions involving only fields Z that are not part of the standard model; an observable sector, which contains all interactions involving only standard model fields and their superpartners; and a mediation sector, which contains all remaining interactions coupling fields Z to the standard model. Supersymmetry is broken in the supersymmetry breaking sector when one or more of the Z fields obtains a non-zero vev: $Z \to F$. This is then transmitted to the observable fields through the mediating interactions. In contrast to the case of EWSB, the supersymmetry-breaking vev F has mass dimension 2. (It is the vev of the auxiliary field of the Z supermultiplet.)

In simple cases where only one non-zero F vev develops, the gravitino mass is

$$m_{3/2} = \frac{F}{\sqrt{3}M_*}, \tag{8}$$

where $M_* \equiv (8\pi G_N)^{-1/2} \simeq 2.4 \times 10^{18}$ GeV is the reduced Planck mass. The standard model superpartner masses are determined through the mediating interactions by terms such as

$$c_{ij}\frac{Z^\dagger Z}{M_m^2}\tilde{f}_i^*\tilde{f}_j \quad \text{and} \quad c_a\frac{Z}{M_m}\lambda_a\lambda_a, \tag{9}$$

where c_{ij} and c_a are constants, $\tilde{f}_i$ and λ_a are superpartners of standard model fermions and gauge bosons, respectively, and M_m is the mass scale of the mediating interactions. When $Z \to F$, these terms become mass terms for sfermions and gauginos. Assuming order one constants,

$$m_{\tilde{f}}, m_\lambda \sim \frac{F}{M_m}. \tag{10}$$

In supergravity models, the mediating interactions are gravitational, and so $M_m \sim M_*$. We then have

$$m_{3/2}, m_{\tilde{f}}, m_\lambda \sim \frac{F}{M_*}, \tag{11}$$

and $\sqrt{F} \sim \sqrt{M_{\rm weak} M_*} \sim 10^{10}$ GeV. In such models with "high-scale" supersymmetry breaking, the gravitino or any standard model superpartner could in principle be the LSP. In contrast, in "low-scale" supersymmetry breaking models with $M_m \ll M_*$, such as gauge-mediated supersymmetry breaking models,

$$m_{3/2} = \frac{F}{\sqrt{3} M_*} \ll m_{\tilde{f}}, \quad m_\lambda \sim \frac{F}{M_m}, \tag{12}$$

$\sqrt{F} \sim \sqrt{M_{\rm weak} M_m} \ll 10^{10}$ GeV, and the gravitino is necessarily the LSP.

As with electroweak symmetry breaking, the dynamics of supersymmetry breaking contributes to the energy density of the vacuum, that is, to dark energy. In non-supersymmetric theories, the vacuum energy density is presumably naturally $\Lambda \sim M_*^4$ instead of its measured value $\sim$meV^4, a discrepancy of 10^{120}. This is the cosmological constant problem. In supersymmetric theories, the vacuum energy density is naturally F^2. For high-scale supersymmetry breaking, one finds $\Lambda \sim M_{\rm weak}^2 M_*^2$, reducing the discrepancy to 10^{90}. Lowering the supersymmetry breaking scale as much as possible to $F \sim M_{\rm weak}^2$ gives $\Lambda \sim M_{\rm weak}^4$, still a factor of 10^{60} too big. Supersymmetry therefore eliminates from 1/4 to 1/2 of the fine-tuning in the cosmological constant, a truly underwhelming achievement. One must look deeper for insights about dark energy and a solution to the cosmological constant problem.

2.6. Minimal supergravity

To obtain detailed information regarding the superpartner spectrum, one must turn to specific models. These are motivated by the expectation that the weak-scale supersymmetric theory is derived from a more fundamental framework, such as a grand unified theory or string theory, at smaller length scales. This more fundamental theory should be highly structured for at least two reasons. First, unstructured theories lead to violations of low energy constraints, such as bounds on flavor-changing neutral currents and CP-violation in the kaon system and in electric dipole moments. Second, the gauge coupling constants unify at high energies in supersymmetric theories [5], and a more fundamental theory should explain this.

From this viewpoint, the many parameters of weak-scale supersymmetry should be derived from a few parameters defined at smaller length scales through renormalization group evolution. Minimal supergravity [6–10], the canonical model for studies of supersymmetry phenomenology and cosmology, is defined by five parameters:

$$m_0, \quad M_{1/2}, \quad A_0, \quad \tan\beta, \quad \text{sign}(\mu), \tag{13}$$

where the most important parameters are the universal scalar mass m_0 and the universal gaugino mass $M_{1/2}$, both defined at the grand unified scale $M_{\rm GUT} \simeq 2 \times 10^{16}$ GeV. In fact, there is a sixth free parameter, the gravitino mass

$$m_{3/2}. \tag{14}$$

As noted in Section 2.5, the gravitino may naturally be the LSP. It may play an important cosmological role, as we will see in Section 4. For now, however, we follow most of the literature and assume the gravitino is heavy and so irrelevant for most discussions.

The renormalization group evolution of supersymmetry parameters is shown in Fig. 5 for a particular point in minimal supergravity parameter space. This figure illustrates several key features that hold more generally. First, as superpartner masses evolve from $M_{\rm GUT}$ to $M_{\rm weak}$, gauge couplings increase these parameters, while Yukawa couplings decrease them. At the weak scale, colored particles are therefore expected to be heavy, and unlikely to be the LSP. The Bino is typically the lightest gaugino, and the right-handed sleptons (more specifically, the right-handed stau $\tilde{\tau}_{\rm R}$) are typically the lightest scalars.

Second, the mass parameter $m^2_{H_{\rm u}}$ is typically driven negative by the large top Yukawa coupling. This is a requirement for electroweak symmetry breaking: at tree-level, minimization of the electroweak potential at the weak scale requires

$$|\mu|^2 = \frac{m^2_{H_{\rm d}} - m^2_{H_{\rm u}}\tan^2\beta}{\tan^2\beta - 1} - \frac{1}{2}m_Z^2 \approx -m^2_{H_{\rm u}} - \frac{1}{2}m_Z^2, \tag{15}$$

where the last line follows for all but the lowest values of $\tan\beta$, which are phenomenologically disfavored anyway. Clearly, this equation can only be satisfied if $m^2_{H_{\rm u}} < 0$. This property of evolving to negative values is unique to $m^2_{H_{\rm u}}$; all other mass

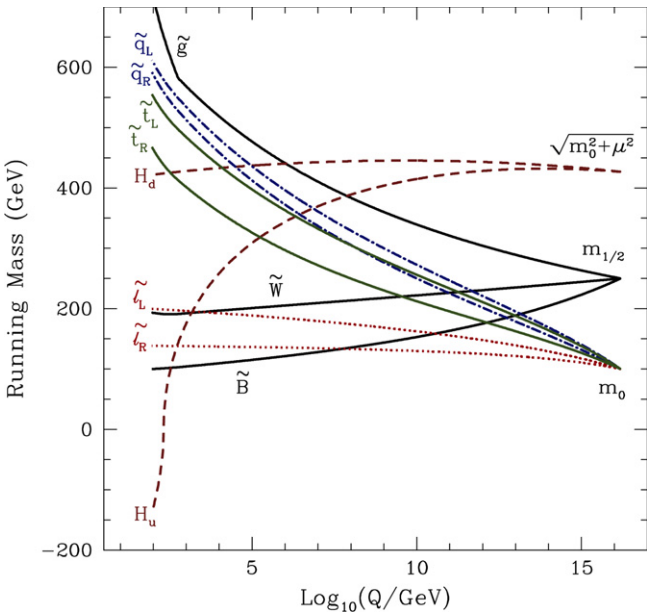

Fig. 5. Renormalization group evolution of supersymmetric mass parameters. From [11].

parameters that are significantly diminished by the top Yukawa coupling also experience a compensating enhancement from the strong gauge coupling. This behavior naturally explains why SU(2) is broken while the other gauge symmetries are not. It is a beautiful feature of supersymmetry derived from a simple high energy framework and lends credibility to the extrapolation of parameters all the way up to a large mass scale like $M_{\rm GUT}$.

Given a particular high energy framework, one may then scan parameter space to determine what possibilities exist for the LSP. The results for a slice through minimal supergravity parameter space are shown in Fig. 6. They are not surprising. The LSP is either the the lightest neutralino χ or the right-handed stau $\tilde{\tau}_{\rm R}$. In the χ LSP case, contours of gaugino-ness

$$R_\chi \equiv |a_{\tilde{B}}|^2 + |a_{\tilde{W}}|^2, \tag{16}$$

where

$$\chi = a_{\tilde{B}}(-\mathrm{i}\tilde{B}) + a_{\tilde{W}}(-\mathrm{i}\tilde{W}) + a_{\tilde{H}_{\rm d}}\tilde{H}_{\rm d} + a_{\tilde{H}_{\rm u}}\tilde{H}_{\rm u}, \tag{17}$$

are also shown. The neutralino is nearly pure Bino in much of parameter space, but may have a significant Higgsino mixture for $m_0 \gtrsim 1$ TeV, where Eq. (15) implies $|\mu| \sim M_1$.

There are, of course, many other models besides minimal supergravity. Phenomena that do not occur in minimal supergravity may very well occur or even be generic in other supersymmetric frameworks. On the other hand, if one looks hard enough,

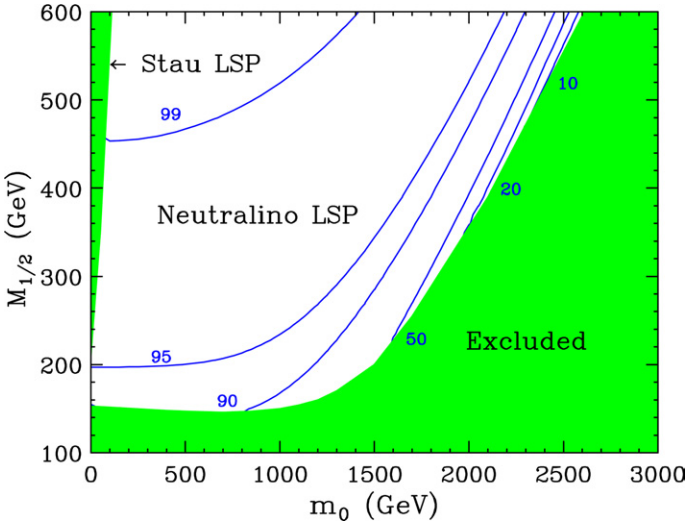

Fig. 6. Regions of the $(m_0, M_{1/2})$ parameter space in minimal supergravity with $A_0 = 0$, $\tan\beta = 10$, and $\mu > 0$. The lower shaded region is excluded by the LEP chargino mass limit. The stau is the LSP in the narrow upper shaded region. In the rest of parameter space, the LSP is the lightest neutralino, and contours of its gaugino-ness R_χ (in percent) are shown. From [12].

minimal supergravity contains a wide variety of dark matter possibilities, and it will serve as a useful framework for illustrating many points below.

2.7. Summary

- Supersymmetry is a new spacetime symmetry that predicts the existence of a new boson for every known fermion, and a new fermion for every known boson.
- The gauge hierarchy problem may be solved by supersymmetry, but requires that all superpartners have masses at the weak scale.
- The introduction of superpartners at the weak scale mediates proton decay at unacceptably large rates unless some symmetry is imposed. An elegant solution, R-parity conservation, implies that the LSP is stable. Electrically neutral superpartners, such as the neutralino and gravitino, are therefore promising dark matter candidates.
- The superpartner masses depend on how supersymmetry is broken. In models with high-scale supersymmetry breaking, such as supergravity, the gravitino may or may not be the LSP; in models with low-scale supersymmetry breaking, the gravitino is the LSP.
- Among standard model superpartners, the lightest neutralino naturally emerges as the dark matter candidate from the simple high energy framework of minimal supergravity.
- Supersymmetry reduces fine tuning in the cosmological constant from 1 part in 10^{120} to 1 part in 10^{60} to 10^{90}, and so does not provide much insight into the problem of dark energy.

3. Neutralino cosmology

Given the motivations described in Section 2 for stable neutralino LSPs, it is natural to consider the possibility that neutralinos are the dark matter [13–15]. In this section, we review the general formalism for calculating thermal relic densities and its implications for neutralinos and supersymmetry. We then describe a few of the more promising methods for detecting neutralino dark matter.

3.1. Freeze out and WIMPs

Dark matter may be produced in a simple and predictive manner as a thermal relic of the Big Bang. The very early universe is a very simple place—all particles are in thermal equilibrium. As the universe cools and expands, however, interaction rates become too low to maintain this equilibrium, and so particles "freeze out." Unstable particles that freeze out disappear from the universe. However, the number of stable particles asymptotically approaches a non-vanishing constant, and this, their thermal relic density, survives to the present day.

This process is described quantitatively by the Boltzmann equation

$$\frac{dn}{dt} = -3Hn - \langle \sigma_A v \rangle (n^2 - n_{eq}^2), \tag{18}$$

where n is the number density of the dark matter particle χ, H is the Hubble parameter, $\langle \sigma_A v \rangle$ is the thermally averaged annihilation cross-section, and n_{eq} is the χ number density in thermal equilibrium. On the right-hand side of Eq. (18), the first term accounts for dilution from expansion. The n^2 term arises from processes $\chi\chi \to f\bar{f}$ that destroy χ particles, and the n_{eq}^2 term arises from the reverse process $f\bar{f} \to \chi\chi$, which creates χ particles.

It is convenient to change variables from time to temperature,

$$t \to x \equiv \frac{m}{T}, \tag{19}$$

where m is the χ mass, and to replace the number density by the co-moving number density

$$n \to Y \equiv \frac{n}{s}, \tag{20}$$

where s is the entropy density. The expansion of the universe has no effect on Y, because s scales inversely with the volume of the universe when entropy is conserved. In terms of these new variables, the Boltzmann equation is

$$\frac{x}{Y_{eq}} \frac{dY}{dx} = -\frac{n_{eq} \langle \sigma_A v \rangle}{H} \left(\frac{Y^2}{Y_{eq}^2} - 1 \right). \tag{21}$$

In this form, it is clear that before freeze out, when the annihilation rate is large compared with the expansion rate, Y tracks its equilibrium value Y_{eq}. After freeze out, Y approaches a constant. This constant is determined by the annihilation cross-section $\langle \sigma_A v \rangle$. The larger this cross-section, the longer Y follows its exponentially decreasing equilibrium value, and the lower the thermal relic density. This behavior is shown in Fig. 7.

Let us now consider WIMPs—weakly interacting massive particles with mass and annihilation cross-section set by the weak scale: $m^2 \sim \langle \sigma_A v \rangle^{-1} \sim M_{weak}^2$. Freeze out takes place when

$$n_{eq} \langle \sigma_A v \rangle \sim H. \tag{22}$$

Neglecting numerical factors, $n_{eq} \sim (mT)^{3/2} e^{-m/T}$ for a non-relativistic particle, and $H \sim T^2/M_*$. From these relations, we find that WIMPs freeze out when

$$\frac{m}{T} \sim \ln \left[\langle \sigma_A v \rangle m M_* \left(\frac{m}{T} \right)^{1/2} \right] \sim 30. \tag{23}$$

Since $\frac{1}{2}mv^2 = \frac{3}{2}T$, WIMPs freeze out with velocity $v \sim 0.3$.

One might think that, since the number density of a particle falls exponentially once the temperature drops below its mass, freeze out should occur at $T \sim m$. This is not the case. Because gravity is weak and M_* is large, the expansion rate is extremely slow, and freeze out occurs much later than one might naively expect. For a

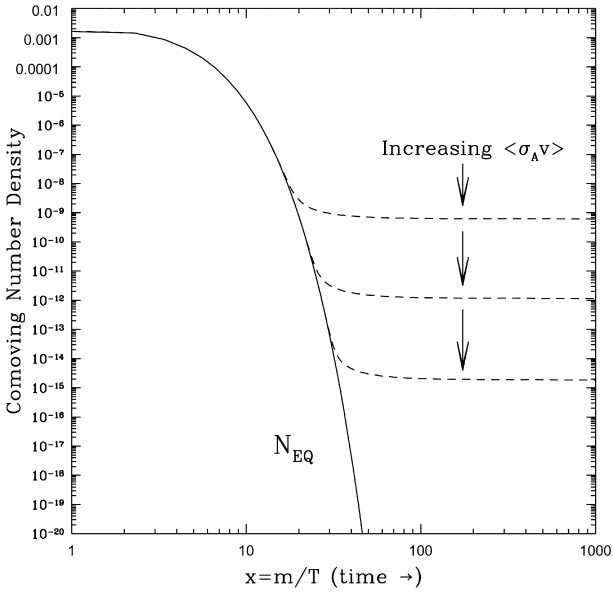

Fig. 7. The co-moving number density Y of a dark matter particle as a function of temperature and time. From [16].

$m \sim 300$ GeV particle, freeze out occurs not at $T \sim 300$ GeV and time $t \sim 10^{-12}$ s, but rather at temperature $T \sim 10$ GeV and time $t \sim 10^{-8}$ s.

With a little more work [17], one can find not just the freeze out time, but also the freeze out density

$$\Omega_\chi = msY(x = \infty) \sim \frac{10^{-10}\ \text{GeV}^{-2}}{\langle \sigma_{\text{A}} v \rangle}. \tag{24}$$

A typical weak cross-section is

$$\langle \sigma_{\text{A}} v \rangle \sim \frac{\alpha^2}{M^2_{\text{weak}}} \sim 10^{-9}\ \text{GeV}^{-2}, \tag{25}$$

corresponding to a thermal relic density of $\Omega h^2 \sim 0.1$. WIMPs therefore naturally have thermal relic densities of the observed magnitude. The analysis above has ignored many numerical factors, and the thermal relic density may vary by as much as a few orders of magnitude. Nevertheless, in conjunction with the other strong motivations for new physics at the weak scale, this coincidence is an important hint that the problems of electroweak symmetry breaking and dark matter may be intimately related.

3.2. Thermal relic density

We now want to apply the general formalism above to the specific case of neutralinos. This is complicated by the fact that neutralinos may annihilate to many final

states: $f\bar{f}$, W^+W^-, ZZ, Zh, hh, and states including the heavy Higgs bosons H, A, and $H^\pm$. Many processes contribute to each of these final states, and nearly every supersymmetry parameter makes an appearance in at least one process. The full set of annihilation diagrams is discussed in [18]. Codes to calculate the relic density are publicly available [19].

Given this complicated picture, it is not surprising that there are a variety of ways to achieve the desired relic density for neutralino dark matter. What is surprising, however, is that many of these different ways may be found in minimal supergravity, provided one looks hard enough. We will therefore consider various regions of minimal supergravity parameter space where qualitatively distinct mechanisms lead to neutralino dark matter with the desired thermal relic density.

3.2.1. Bulk region

As evident from Fig. 6, the LSP is a Bino-like neutralino in much of minimal supergravity parameter space. It is useful, therefore, to begin by considering the pure Bino limit. In this case, all processes with final state gauge bosons vanish. This follows from supersymmetry and the absence of 3-gauge boson vertices involving the hypercharge gauge boson.

The process $\chi\chi \to f\bar{f}$ through a t-channel sfermion does not vanish in the Bino limit. This process is the first shown in Fig. 8. This reaction has an interesting structure. Recall that neutralinos are Majorana fermions. If the initial state neutralinos are in an S-wave state, the Pauli exclusion principle implies that the initial state is CP-odd, with total spin $S = 0$ and total angular momentum $J = 0$. If the neutralinos are gauginos, the vertices preserve chirality, and so the final state $f\bar{f}$ has spin $S = 1$. This is compatible with $J = 0$ only with a mass insertion on the fermion line. This process is therefore either P-wave-suppressed (by a factor $v^2 \sim 0.1$) or chirality suppressed (by a factor m_f/M_W). In fact, this conclusion holds also for mixed gaugino-

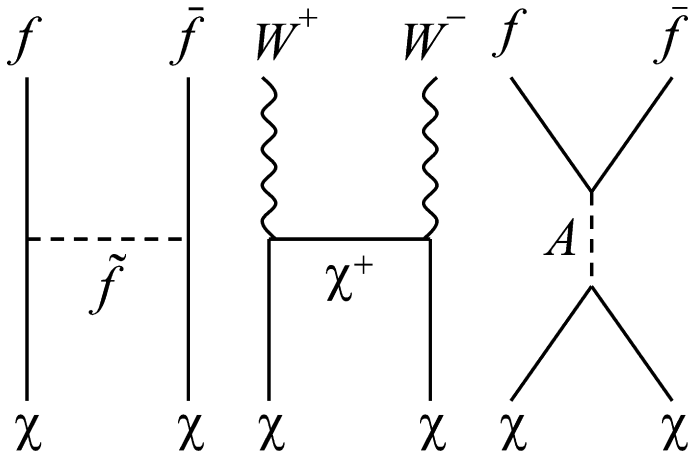

Fig. 8. Three representative neutralino annihilation diagrams.

Higgsino neutralinos and for all other processes contributing to the $f\bar{f}$ final state [18]. (It also has important implications for indirect detection. See Section 3.4.)

The region of minimal supergravity parameter space with a Bino-like neutralino where $\chi\chi \to f\bar{f}$ yields the right relic density is the $(m_0, M_{1/2}) \sim (100\ \text{GeV}, 200\ \text{GeV})$ region shown in Fig. 9. It is called the "bulk region," as, in the past, there was a wide range of parameters with m_0, $M_{1/2} \lesssim 300$ GeV that predicted dark matter within the observed range. The dark matter energy density has by now become so tightly constrained, however, that the "bulk region" has now been reduced to a thin ribbon of acceptable parameter space.

Moving from the bulk region by increasing m_0 and keeping all other parameters fixed, one finds too much dark matter. This behavior is evident in Fig. 9 and not difficult to understand: in the bulk region, a large sfermion mass suppresses $\langle \sigma_{\text{Av}} \rangle$, which implies a large Ω_{DM}. In fact, sfermion masses not far above current bounds are required to offset the P-wave suppression of the annihilation cross-section. This is an interesting fact—cosmology seemingly provides an upper bound on superpartner masses! If this were true, one could replace subjective naturalness arguments by

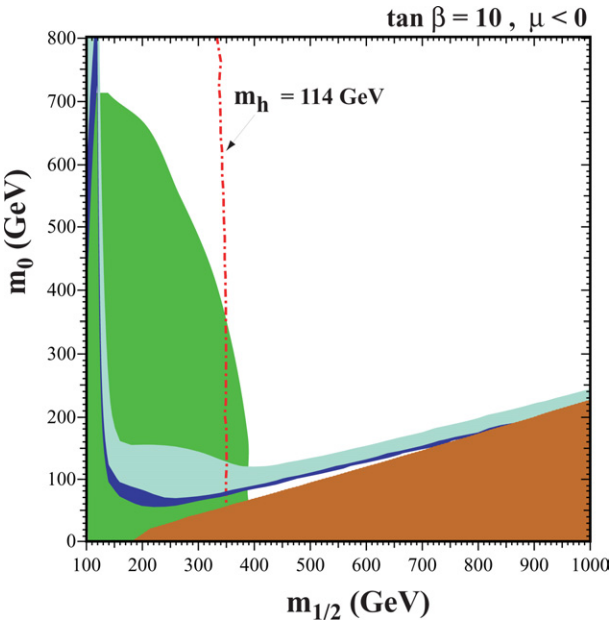

Fig. 9. The bulk and co-annihilation regions of minimal supergravity with $A_0 = 0$, $\tan\beta = 10$ and $\mu < 0$. In the light blue region, the thermal relic density satisfies the pre-WMAP constraint $0.1 < \Omega_{\text{DM}}h^2 < 0.3$. In the dark blue region, the neutralino density is in the post-WMAP range $0.094 < \Omega_{\text{DM}}h^2 < 0.129$. The bulk region is the dark blue region with $(m_0, M_{1/2}) \sim (100\ \text{GeV}, 200\ \text{GeV})$. The stau LSP region is given in dark red, and the co-annihilation region is the dark blue region along the stau LSP border. Current bounds on $b \to s\gamma$ exclude the green shaded region, and the Higgs mass is too low to the left of the $m_h = 114$ GeV contour. From [20].

the fact that the universe cannot be overclosed to provide upper bounds on superpartner masses.

Unfortunately, this line of reasoning is not airtight even in the constrained framework of minimal supergravity. The discussion above assumes that $\chi\chi \to f\bar{f}$ is the only annihilation channel. In fact, however, for non-Bino-like neutralinos, there are many other contributions. Exactly this possibility is realized in the focus point region, which we describe next.

In passing, it is important to note that the bulk region, although the most straightforward and natural in many respects, is also severely constrained by other data. The existence of a light superpartner spectrum in the bulk region implies a light Higgs boson mass, and typically significant deviations in low energy observables such as $b \to s\gamma$ and $(g-2)_\mu$. Current bounds on the Higgs boson mass, as well as concordance between experiments and standard model predictions for $b \to s\gamma$ and (possibly) $(g-2)_\mu$, therefore disfavor this region, as can be seen in Fig. 9. For this reason, it is well worth considering other possibilities, including the three we now describe.

3.2.2. Focus point region

As can be seen in Fig. 6, a Bino-like LSP is not a definitive prediction of minimal supergravity. For large scalar mass parameter m_0, the Higgsino mass parameter $|\mu|$ drops to accommodate electroweak symmetry breaking, as required by Eq. (15). The LSP then becomes a gaugino-Higgsino mixture. The region where this happens is called the focus point region, a name derived from peculiar properties of the renormalization group equations which suggest that large scalar masses do not necessarily imply fine-tuning [21–23].

In the focus point region, the first diagram of Fig. 8 is suppressed by very heavy sfermions. However, the existence of Higgsino components in the LSP implies that diagrams like the 2nd of Fig. 8, $\chi\chi \to W^+W^-$ through a t-channel chargino, are no longer suppressed. This provides a second method by which neutralinos may annihilate efficiently enough to produce the desired thermal relic density. The cosmologically preferred regions with the right relic densities are shown in Fig. 10. The right amount of dark matter can be achieved with arbitrarily heavy sfermions, and so there is no useful cosmological upper bound on superpartner masses, even in the framework of minimal supergravity.

3.2.3. A funnel region

A third possibility realized in minimal supergravity is that the dark matter annihilates to fermion pairs through an s-channel pole. The potentially dominant process is through the A Higgs boson (the last diagram of Fig. 8), as the A is CP-odd, and so may couple to an initial S-wave state. This process is efficient when $2m_\chi \approx m_A$. In fact, the A resonance may be broad, extending the region of parameter space over which this process is important.

The A resonance region occurs in minimal supergravity for $\tan\beta \gtrsim 40$ [24,25] and is shown in Fig. 11. Note that the resonance is so efficient that the relic density may be reduced too much. The desired relic density is therefore obtained when the process is near resonance, but not exactly on it.

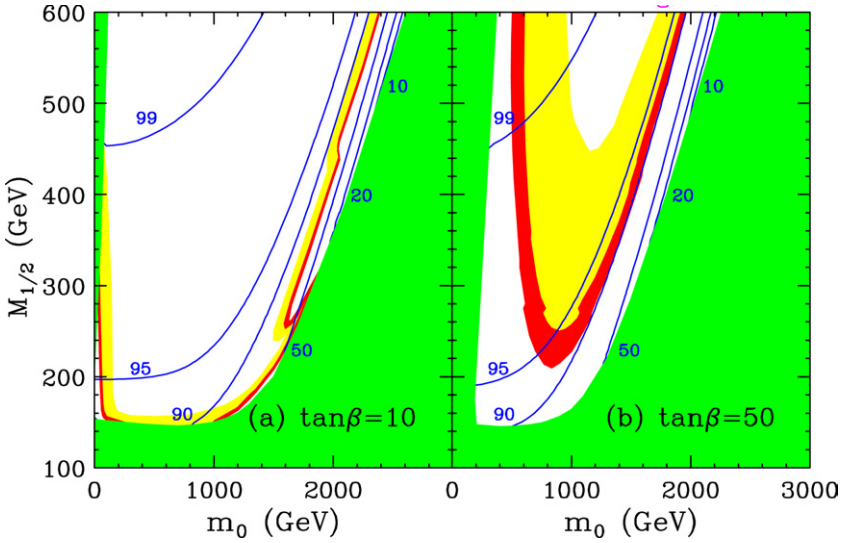

Fig. 10. Focus point region of minimal supergravity for $A_0 = 0$, $\mu > 0$, and $\tan\beta$ as indicated. The excluded regions and contours are as in Fig. 6. In the light yellow region, the thermal relic density satisfies the pre-WMAP constraint $0.1 < \Omega_{\rm DM}h^2 < 0.3$. In the medium red region, the neutralino density is in the post-WMAP range $0.094 < \Omega_{\rm DM}h^2 < 0.129$. The focus point region is the cosmologically favored region with $m_0 \gtrsim 1$ TeV. Updated from [12]. (For interpretation of the references to color in this figure legend, the reader is referred to the web version of this paper.)

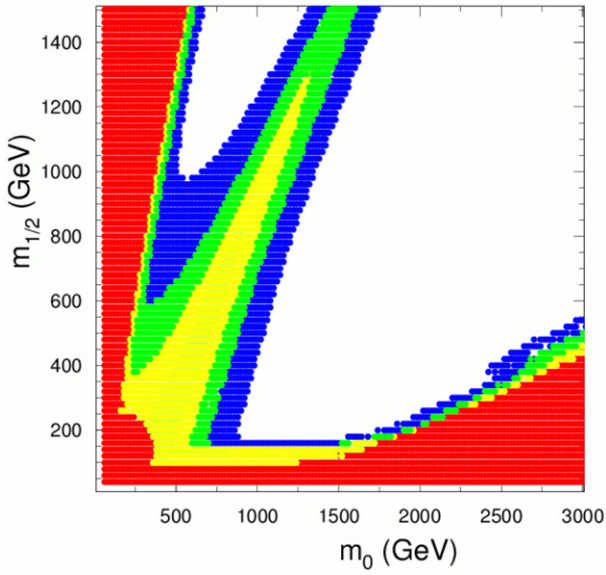

Fig. 11. The A funnel region of minimal supergravity with $A_0 = 0$, $\tan\beta = 45$, and $\mu < 0$. The red region is excluded. The other shaded regions have $\Omega_{\rm DM}h^2 < 0.1$ (yellow), $0.1 < \Omega_{\rm DM}h^2 < 0.3$ (green), and $0.3 < \Omega_{\rm DM}h^2 < 1$ (blue). From [25]. (For interpretation of the references to color in this figure legend, the reader is referred to the web version of this paper.)

3.2.4. Co-annihilation region

Finally, the desired neutralino relic density may be obtained even if $\chi\chi$ annihilation is inefficient if there are other particles present in significant numbers when the LSP freezes out. The neutralino density may then be brought down through co-annihilation with the other species [26,27]. Naively, the presence of other particles requires that they be mass degenerate with the neutralino to within the temperature at freeze out, $T \approx m_\chi/30$. In fact, co-annihilation may be so enhanced relative to the P-wave-suppressed $\chi\chi$ annihilation cross section that co-annihilation may be important even with mass splittings much larger than T.

The co-annihilation possibility is realized in minimal supergravity along the $\tilde{\tau}$ LSP—χ LSP border (see Fig. 9). Processes such as $\chi\tilde{\tau} \to \tau^* \to \tau\gamma$ are not P-wave suppressed, and so enhance the $\chi\chi$ annihilation rate substantially. There is therefore a narrow finger extending up to masses $m_\chi \sim 600$ GeV with acceptable neutralino thermal relic densities.

3.3. Direct detection

If dark matter is composed of neutralinos, it may be detected directly, that is, by looking for signals associated with its scattering in ordinary matter. Dark matter velocity and spatial distributions are rather poorly known and are an important source of uncertainty [28–32]. A common assumption is that dark matter has a local energy density of $\rho_\chi = 0.3\ \text{GeV/cm}^3$ with a velocity distribution characterized by a velocity $v \approx 220$ km/s. Normalizing to these values, the neutralino flux is

$$\Phi_\chi = 6.6 \times 10^4\ \text{cm}^{-2}\ \text{s}^{-1} \frac{\rho_\chi}{0.3\ \text{GeV/cm}^3} \frac{100\ \text{GeV}}{m_\chi} \frac{v}{220\ \text{km/s}}. \tag{26}$$

Such values therefore predict a substantial flux of halo neutralinos in detectors here on Earth.

The maximal recoil energy from a WIMP scattering off a nucleus N is

$$E_{\text{recoil}}^{\max} = \frac{2m_\chi^2 m_N}{(m_\chi + m_N)^2} v^2 \sim 100\ \text{keV}. \tag{27}$$

With such low energies, elastic scattering is the most promising signal at present, although the possibility of detecting inelastic scattering has also been discussed. As we will see below, event rates predicted by supersymmetry are at most a few per kilogram per day. Neutralino dark matter therefore poses a serious experimental challenge, requiring detectors sensitive to extremely rare events with low recoil energies.

Neutralino–nucleus interactions take place at the parton level through neutralino–quark interactions, such as those in Fig. 12. Because neutralinos now have velocities $v \sim 10^{-3}$, we may take the non-relativistic limit for these scattering amplitudes. In this limit, only two types of neutralino-quark couplings are non-vanishing [33]. The interaction Lagrangian may be parameterized as

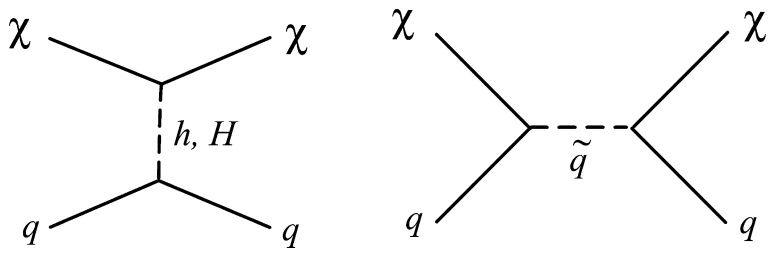

Fig. 12. Feynman diagrams contributing to $\chi q \to \chi q$ scattering.

$$\mathscr{L} = \sum_{q=u,d,s,c,b,t} \left(\alpha_q^{\mathrm{SD}} \bar{\chi}\gamma^\mu\gamma^5\chi\bar{q}\gamma_\mu\gamma^5 q + \alpha_q^{\mathrm{SI}} \bar{\chi}\chi\bar{q}q \right). \tag{28}$$

The first term is the spin-dependent coupling, as it reduces to $\boldsymbol{S}_\chi \cdot \boldsymbol{S}_N$ in the non-relativistic limit. The second is the spin-independent coupling. All of the supersymmetry model dependence is contained in the parameters α_q^{SD} and α_q^{SI}. The t-channel Higgs exchange diagram of Fig. 12 contributes solely to α_q^{SI}, while the s-channel squark diagram contributes to both α_q^{SD} and α_q^{SI}.

For neutralinos scattering off protons, the spin-dependent coupling is dominant. However, the spin-independent coupling is coherent and so greatly enhanced for heavy nuclei, a fact successfully exploited by current experiments. As a result, spin-independent direct detection is currently the most promising approach for neutralino dark matter, and we focus on this below.

Given the parameters α_q^{SI}, the spin-independent cross-section for χN scattering is

$$\sigma_{\mathrm{SI}} = \frac{4}{\pi}\mu_N^2 \sum_q {\alpha_q^{\mathrm{SI}}}^2 \left[Z\frac{m_p}{m_q} f_{T_q}^p + (A-Z)\frac{m_n}{m_q} f_{T_q}^n \right]^2, \tag{29}$$

where

$$\mu_N = \frac{m_\chi m_N}{m_\chi + m_N} \tag{30}$$

is the reduced mass of the $\chi - N$ system, Z and A are the atomic number and weight of the nucleus, respectively, and

$$f_{T_q}^{p,n} = \frac{\langle p,n|m_q\bar{q}q|p,n\rangle}{m_{p,n}} \tag{31}$$

are constants quantifying what fraction of the nucleon's mass is carried by quark q. For the light quarks [34],

$$\begin{aligned} f_{T_{\mathrm{u}}}^p &= 0.020 \pm 0.004, \quad f_{T_{\mathrm{u}}}^n = 0.014 \pm 0.003, \\ f_{T_{\mathrm{d}}}^p &= 0.026 \pm 0.005, \quad f_{T_{\mathrm{d}}}^n = 0.036 \pm 0.008, \\ f_{T_s}^p &= 0.118 \pm 0.062, \quad f_{T_s}^n = 0.118 \pm 0.062. \end{aligned} \tag{32}$$

The contribution from neutralino-gluon couplings mediated by heavy quark loops may be included by taking $f_{T_{c,b,t}}^{p,n} = \frac{2}{27} f_{T_G}^{p,n} = \frac{2}{27}(1 - f_{T_{\mathrm{u}}}^{p,n} - f_{T_{\mathrm{d}}}^{p,n} - f_{T_s}^{p,n})$ [35].

The number of dark matter scattering events is

$$\mathcal{N} = N_N T \frac{\rho_\chi}{m_\chi} \sigma_N v \tag{33}$$

$$= 3.4 \times 10^{-6} \frac{M_D}{\text{kg}} \frac{T}{\text{day}} \frac{\rho_\chi}{0.3\ \text{GeV/cm}^3} \frac{100\ \text{GeV}}{m_\chi} \frac{v}{220\ \text{km/s}} \frac{\mu_N^2 A}{m_p^2} \frac{\sigma_p}{10^{-6}\ \text{pb}}, \tag{34}$$

where N_N is the number of target nuclei, T is the experiment's running time, M_D is the mass of the detector, and the proton scattering cross-section σ_p has been normalized to a near-maximal supersymmetric value. This is a discouragingly low event rate. However, for a detector with a fixed mass, this rate is proportional to $\mu_N^2 A$. For heavy nuclei with $A \sim m_\chi/m_p$, the event rate is enhanced by a factor of $\sim A^3$, providing the strong enhancement noted above.

Comparisons between theory and experiment are typically made by converting all results to proton scattering cross-sections. In Fig. 13, minimal supergravity predictions for spin-independent cross sections are given. These vary by several orders of magnitude. In the stau co-annihilation region, these cross sections can be small, as the neutralino is Bino-like, suppressing the Higgs diagram, and squarks can be quite heavy, suppressing the squark diagram. However, in the focus point region, the neutralino is a gaugino-Higgsino mixture, and the Higgs diagram is large. Current and projected experimental sensitivities are also shown in Fig. 13. Current

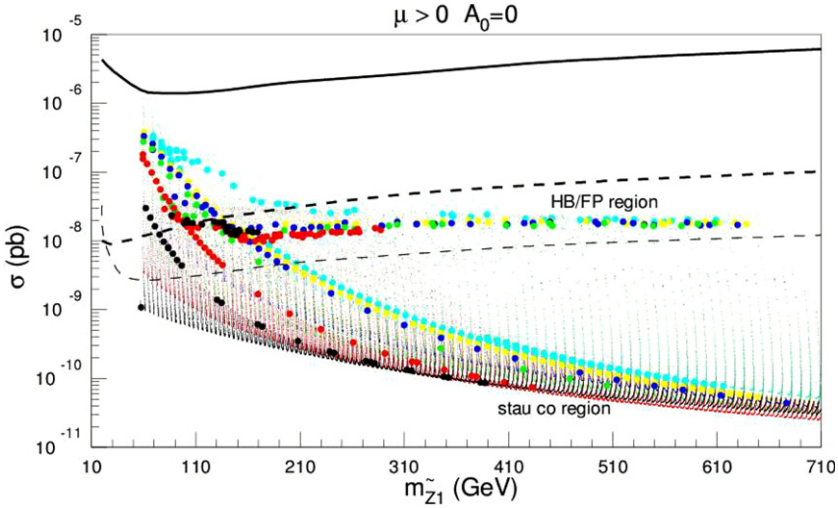

Fig. 13. Spin-independent neutralino-proton cross-sections for minimal supergravity models with $A_0 = 0$, $\mu > 0$. The colors correspond to various values of $\tan\beta$ in the range $10 \leqslant \tan\beta \leqslant 55$. Points with the preferred thermal relic density $0.094 < \Omega_{\text{DM}} h^2 < 0.129$ are highlighted with enlarged circles, and those in the focus point and co-annihilation regions are indicated. Estimated reaches of current (CDMS, EDELWEISS, ZEPLIN1, and DAMA), near future (CDMS2, EDELWEISS2, ZEPLIN2, and CRESST2), and future detectors (GENIUS, ZEPLIN4, and CRYOARRAY) are given by the solid, dark dashed, and light dashed contours, respectively. From [36].

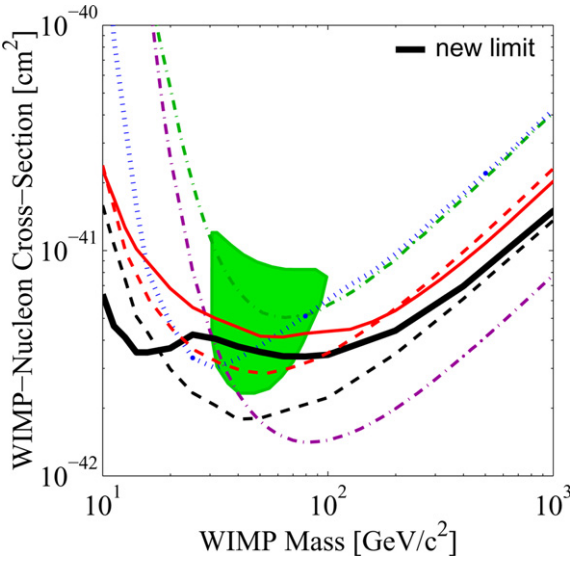

Fig. 14. Regions of dark matter mass and spin-independent proton scattering cross-sections. The shaded region is the 3σ favored region from DAMA. The dot-dashed line is the exclusion contour from EDELWEISS, and the thick solid black line is the exclusion contour from CDMS. From [39].

experiments are just now probing the interesting parameter region for supersymmetry, but future searches will provide stringent tests of some of the more promising minimal supergravity predictions.

The DAMA collaboration has reported evidence for direct detection of dark matter from annual modulation in scattering rates [37]. The favored dark matter mass and proton spin-independent cross section are shown in Fig. 14. By comparing Figs. 13 and 14, one sees that the interaction strength favored by DAMA is very large relative to typical predictions in minimal supergravity. Such cross sections may be realized in less restrictive supersymmetry scenarios. However, more problematic from the point of view of providing a supersymmetric interpretation is that the experiments EDELWEISS [38] and CDMS [39] have also searched for dark matter with similar sensitivities and have not found signals. Their exclusion bounds are also given in Fig. 14.[1] Given standard halo and neutralino interaction assumptions, these data are inconsistent at a high level.

Non-standard halo models and velocity distributions [41,42] and non-standard and generalized dark matter interactions [43–46] have been considered as means to bring consistency to the experimental picture. The results are mixed. Given the current status of direct detection experiments, a supersymmetric interpretation is at best premature. It is worth noting, however, that the current results bode well for the

[1] Recent data from CDMS in the Soudan mine has pushed the discrepancy to even greater levels [40].

future, as many well-motivated supersymmetry models predict cross sections not far from current sensitivities.

3.4. Indirect detection

After freeze out, dark matter pair annihilation becomes greatly suppressed. However, after the creation of structure in the universe, dark matter annihilation in overdense regions of the universe may again become significant. Dark matter may therefore be detected indirectly: pairs of dark matter particles annihilate *somewhere*, producing *something*, which is detected *somehow*. There are a large number of possibilities. Below we briefly discuss three of the more promising signals.

3.4.1. Positrons

Dark matter in our galactic halo may annihilate to positrons, which may be detected in space-based or balloon-borne experiments [47–52]. (Anti-protons [53–56] and anti-deuterium [57] have also been suggested as promising signals.)

The positron background is most likely to be composed of secondaries produced in the interactions of cosmic ray nuclei with interstellar gas, and is expected to fall as $\sim E_{e^+}^{-3.1}$. At energies below 10 GeV, there are also large uncertainties in the background [51,52]. The most promising signal is therefore hard positrons from $\chi\chi$ annihilation.

Unfortunately, the monoenergetic signal $\chi\chi \to e^+e^-$ is extremely suppressed. As noted above, $\chi\chi \to f\bar{f}$ is either P-wave suppressed or chirality suppressed. At present times, as opposed to during freeze out, P-wave suppression is especially severe, since $v^2 \sim 10^{-6}$, and so direct annihilation to positrons is effectively absent.[2] The positron signal therefore results from processes such as $\chi\chi \to W^+W^-$ followed by $W^+ \to e^+\nu$, and is a continuum, not a line, at the source.

To obtain the positron energy distribution we would observe, the source energy distribution must be propagated through the halo to us. The resulting differential positron flux is [52]

$$\frac{\mathrm{d}\Phi_{e^+}}{\mathrm{d}\Omega\,\mathrm{d}E} = \frac{\rho_\chi^2}{m_\chi^2}\sum_i \sigma_i v B_{e^+}^i \int \mathrm{d}E_0\, f_i(E_0)\, G(E_0, E), \tag{35}$$

where ρ_χ is the local neutralino mass density, the sum is over all annihilation channels, and $B_{e^+}^i$ is the branching fraction to positrons in channel i. The source function $f(E_0)$ gives the initial positron energy distribution from neutralino annihilation. $G(E_0, E)$ is the Green's function describing positron propagation in the galaxy [60] and contains all the halo model dependence.

Three sample positron spectra are given in Fig. 15. For all of them, $E^2\mathrm{d}\Phi/\mathrm{d}E$ peaks at energies $E \sim m_\chi/2$. These signals are all well below background. However, a smooth halo distribution has been assumed. For clumpy halos, which are well

[2] Note that this suppression is rather special, in that it follows from the Majorana nature of neutralinos; it is absent for other types of dark matter, such as dark matter with spin 1 [58,59].

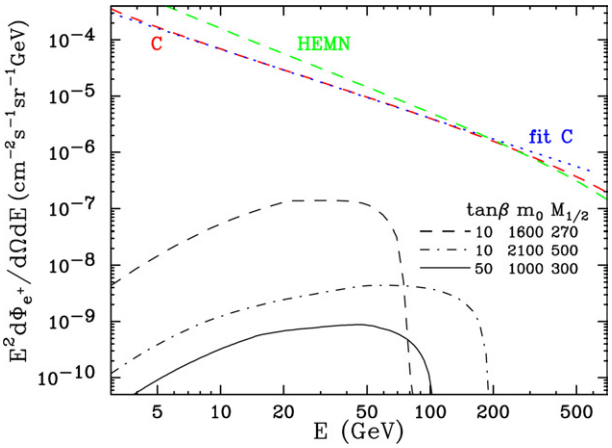

Fig. 15. The differential positron flux for three minimal supergravity models. The curves labeled C and HEMN are background models from [52]. From [95].

within the realm of possibility, the signal may be enhanced significantly. In the next few years, both PAMELA, a satellite detector, and AMS-02, an experiment to be placed on the International Space Station, will provide precision probes of the positron spectrum. These experiments and other recently completed experiments are listed in Table 1.

Finally, the high energy antimatter telescope (HEAT) experiment, a balloon-borne magnetic spectrometer, has found evidence for an excess of positrons at energy ~8 GeV in data from 1994/95 [61,62] and 2000 [63]. The observed bump in the positron fraction $N_{e^+}/(N_{e^+}+N_{e^-})$ is not naturally obtained by neutralino dark matter for two reasons. First, as noted above, for a smooth halo, the annihilation cross sections that produce the desired relic density predict positron fluxes that are far too low to explain the observed excess. In principle, this objection may be overcome by a sufficiently clumpy halo. Second, neutralino annihilation produces positrons only through cascades, resulting in a smooth positron energy distribution. This is an inevitable consequence of the Majorana nature of neutralinos. Nevertheless, even the addition of a smooth component from neutralino annihilation may improve the fit to data, and the possibility of a supersymmetric explanation for the HEAT anomaly has been explored in a number of studies [64–66].

Table 1
Recent and planned e^+ detector experiments

Experiment	Type	Date	Duration	Accept	$E_{e^+}^{\max}$	$\frac{dN}{dE}(100)$
HEAT94/95	Balloon	1994/95	29/26 h	495	50	—
CAPRICE94/98	Balloon	1994/98	18/21 h	163	10/30	—
PAMELA	Satellite		3 yr	20	200	0.7
AMS-02	ISS		3 yr	6500	1000	250

We list each experiment's start date, duration, geometrical acceptance in cm^2 sr, maximal E_{e^+} sensitivity in GeV, and (expected) total number of e^+ detected per GeV at $E_{e^+} = 100$ GeV. From [95].

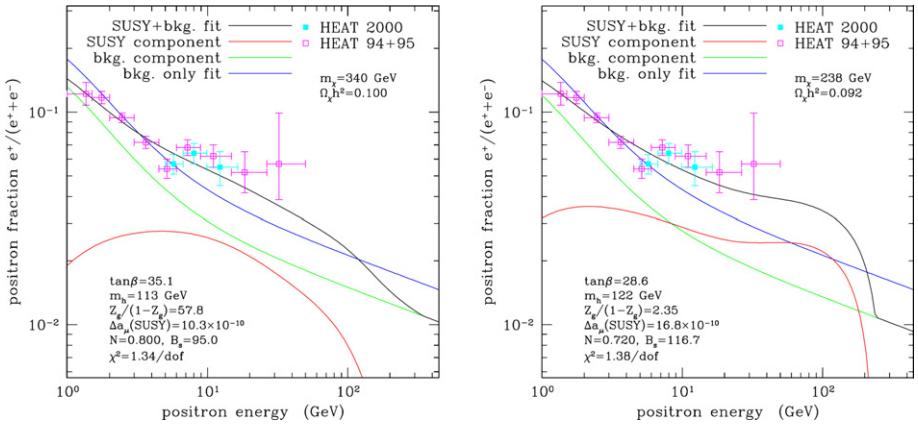

Fig. 16. Two positron spectra for which contributions from neutralino annihilation improve the fit to HEAT data. In each case, the contribution from neutralino annihilation has been enhanced by a factor $B_s \sim 100$ relative to the prediction for a smooth halo. From [65].

Two "best fit" results from [65] are shown in Fig. 16. In this study, the ignorance of subhalo structure is parameterized by a constant B_s, an overall normalization factor that enhances the positron flux relative to what would be expected for a smooth halo. As can be seen in Fig. 16, both spectra give improved fits to the data. They require substantial boost factors, however, with $B_s \sim 100$. Such large boost factors may be disfavored by models of halo formation [67].

3.4.2. Photons

Dark matter in the galactic center may annihilate to photons, which can be detected in atmospheric Cherenkov telescopes on the ground, or in space-based detectors [47,68–74]. (Photons from the galactic halo [75,76], or even from extra-galactic sources [77] have also been considered.)

The main source of photons is from cascade decays of other primary annihilation products. A line source from loop-mediated processes such as $\chi\chi \to \gamma\gamma$ [78–80] and $\chi\chi \to \gamma Z$ [81] is possible [70], but is typically highly suppressed [82].

The differential photon flux along a direction that forms an angle ψ with respect to the direction of the galactic center is

$$\frac{\mathrm{d}\Phi_\gamma}{\mathrm{d}\Omega\,\mathrm{d}E} = \sum_i \frac{\mathrm{d}N_\gamma^i}{\mathrm{d}E}\sigma_i v \frac{1}{4\pi m_\chi^2}\int_\psi \rho^2\,\mathrm{d}l, \tag{36}$$

where the sum is over all annihilation channels, ρ is the neutralino mass density, and the integral is along the line of sight. All of the halo model dependence is isolated in the integral. Depending on the clumpiness or cuspiness of the halo density profile, this integral may vary by as much as 5 orders of magnitude [70].

The integrated photon signal for four representative minimal supergravity models is given in Fig. 17. A moderate halo profile is assumed. Experiments sensitive to such photon fluxes are listed in Table 2, and their sensitivities are given in Fig. 17.

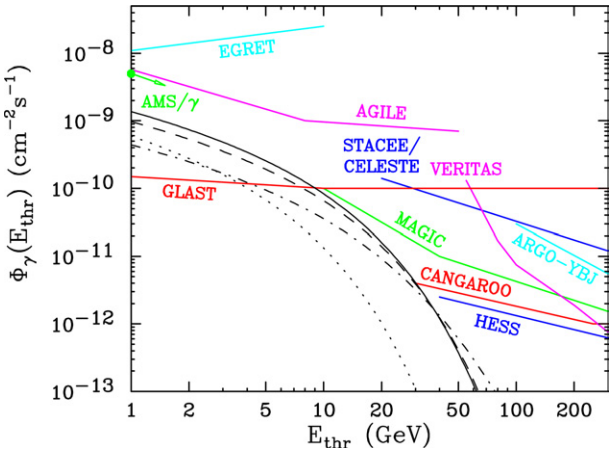

Fig. 17. Integral photon fluxes $\Phi_\gamma(E_{\rm thr})$ as a function of threshold energy $E_{\rm thr}$ for $A_0 = 0$, $\mu > 0$, $m_t = 174$ GeV, and halo parameter $\bar{J} = 500$. The four models have relic density $\Omega_\chi h^2 \approx 0.15$, and are specified by $(\tan\beta, m_0, M_{1/2}, m_\chi, R_\chi) = (10, 100, 170, 61, 0.93)$ (dotted), $(10, 1600, 270, 97, 0.77)$ (dashed), $(10, 2100, 500, 202, 0.88)$ (dot-dashed), and $(50, 1000, 300, 120, 0.96)$ (solid), where all masses are in GeV. Point source flux sensitivity estimates for several gamma ray detectors are also shown. From [95].

Table 2
Some of the current and planned γ ray detector experiments with sensitivity to photon energies 10 GeV $\lesssim E_\gamma \lesssim$ 300 GeV

Experiment	Type	Date	E_γ range
EGRET	Satellite	1991–2000	0.02–30
STACEE	ACT array	1998	20–300
CELESTE	ACT array	1998	20–300
ARGO-YBJ	Air shower	2001	100–2000
MAGIC	ACT		10–1000
AGILE	Satellite		0.03–50
HESS	ACT array		10–1000
AMS/γ	Space station		0.3–100
CANGAROO III	ACT array		30–50,000
VERITAS	ACT array		50–50,000
GLAST	Satellite		0.1–300

We list each experiment's start date and expected E_γ coverage in GeV. The energy ranges are approximate. For experiments constructed in stages, the listed threshold energies will not be realized initially. From [95].

3.4.3. Neutrinos

When neutralinos pass through astrophysical objects, they may be slowed below escape velocity by elastic scattering. Once captured, they then settle to the center, where their densities and annihilation rates are greatly enhanced. While most of their annihilation products are immediately absorbed, neutrinos are not. Neutralinos may therefore annihilate to high energy neutrinos in the cores of the Earth [83–88] and Sun [85,87–94] and be detected on Earth in neutrino telescopes.

The formalism for calculating neutrino fluxes from dark matter annihilation is complicated but well developed (see [16] for a review.) In contrast to the previous two indirect detection examples, neutrino rates depend not only on annihilation cross sections, but also on χN scattering, which determines the neutralino capture rate in the Sun and Earth.

As with positrons, $\chi\chi \to v\bar{v}$ is helicity-suppressed, and so neutrinos are produced only in the decays of primary annihilation products. Typical neutrino energies are then $E_v \sim \frac{1}{2}m_\chi$ to $\frac{1}{3}m_\chi$, with the most energetic spectra resulting from WW, ZZ, and, to a lesser extent, $\tau\bar{\tau}$. After propagating to the Earth's surface, neutrinos are detected through their charged-current interactions. The most promising signal is from upward-going muon neutrinos that convert to muons in the surrounding rock, water, or ice, producing through-going muons in detectors. The detection rate for such neutrinos is greatly enhanced for high energy neutrinos, as both the charged-current cross-section and the muon range are proportional to E_v.

The most promising source of neutrinos is the core of the Sun. Muon flux rates from the Sun are presented in Fig. 18. Fluxes as large as 1000 $\text{km}^{-2}\,\text{s}^{-1}$ are possible. Past, present, and future neutrino telescopes and their properties are listed in Table 3. Comparing Fig. 18 with Table 3, we find that present limits do not significantly constrain the minimal supergravity parameter space. However, given that the effective area of neutrino telescope experiments is expected to increase by 10–100 in the next few years, muon fluxes of order 10–100 $\text{km}^{-2}\,\text{yr}^{-1}$ may be within reach.

3.5. Summary

Neutralinos are excellent dark matter candidates. The lightest neutralino emerges naturally as the lightest supersymmetric particle and is stable in simple supersymmetric models. In addition, the neutralino is non-baryonic, cold, and weakly interacting,

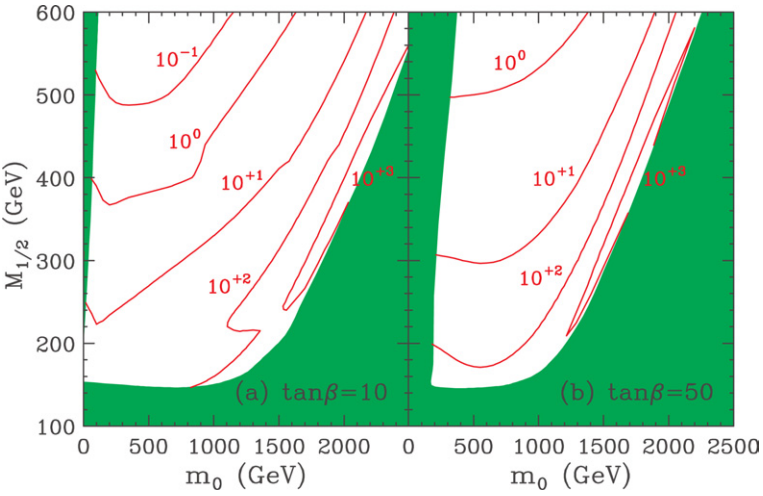

Fig. 18. Muon flux from the Sun in $\text{km}^{-2}\,\text{yr}^{-1}$ for $v = 270$ km/s and $\rho_\chi = 0.3$ GeV/cm^3. From [95]

Table 3
Current and planned neutrino experiments

Experiment	Type	Date	Dimensions	$E_\mu^{\rm thr}$	$\Phi_\mu^\odot$
Baksan	Ground	1978	$17\times17\times11$ m^3	1	7.6×10^3
Kamiokande	Ground	1983	~ 150 m^2	3	17×10^3
MACRO	Ground	1989	$12\times77\times9$ m^3	2	6.5×10^3
Super-Kamiokande	Ground	1996	$\sim$1200 m^2	1.6	5.0×10^3
Baikal NT-96	Water	1996	$\sim$1000 m^2	10	
AMANDA B-10	Under-ice	1997	~ 1000 m^2[a]	$\sim$25	
Baikal NT-200	Water	1998	$\sim$2000 m^2		
AMANDA II	Ice	2000	$\sim3\times10^4$ m^2	$\sim$50	
NESTOR[b]	Water		$\sim10^4$ m^2[c]	Few	
ANTARES	Water		$\sim2\times10^4$ m^2[c]	$\sim$5–10	
IceCube	Ice		$\sim10^6$ m^2		

We list also each experiment's start date, physical dimensions (or approximate effective area), muon threshold energy $E_\mu^{\rm thr}$ in GeV, and 90% CL flux limits for the Sun $\Phi_\mu^\odot$ in km^{-2} yr^{-1} for half-cone angle $\theta\approx15^\circ$ when available. From [95].

[a] Hard spectrum, $m_\chi = 100$ GeV.
[b] One tower.
[c] $E_\mu\sim100$ GeV.

and so has all the right properties to be dark matter, and its thermal relic density is naturally in the desired range.

Current bounds on $\Omega_{\rm DM}$ are already highly constraining. Although these constraints do not provide useful upper bounds on supersymmetric particle masses, they do restrict supersymmetric parameter space. In minimal supergravity, the cosmologically preferred regions of parameter space include the bulk, focus point, A funnel, and stau coannihilation regions.

Neutralinos may be detected either directly through their interactions with ordinary matter or indirectly through their annihilation decay products. Null results from direct and indirect dark matter searches are not yet very constraining. Future sensitivities of various particle physics and dark matter detection experiments are shown in Fig. 19. The sensitivities assumed, and experiments likely to achieve these sensitivities in the near future, are listed in Table 4.

Several interesting features are apparent. First, traditional particle physics and dark matter searches, particularly indirect detection experiments, are highly complementary. Second, at least one dark matter experiment is predicted to see a signal in almost all of the cosmologically preferred region. This illustration is in the context of minimal supergravity, but can be expected to hold more generally. The prospects for neutralino dark matter discovery are therefore promising.

4. Gravitino cosmology

In Section 3, we largely ignored the gravitino. In this section, we will rectify this omission. Although gravitino interactions are highly suppressed, gravitinos may have implications for many aspects of cosmology, including Big Bang nucleosynthe-

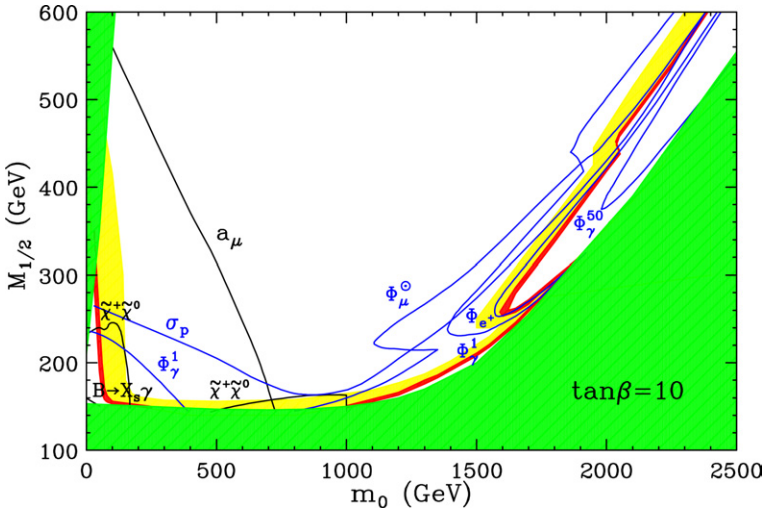

Fig. 19. Estimated reaches of various high-energy collider and low-energy precision searches (black), direct dark matter searches (red), and indirect dark matter searches (blue) in the next few years for minimal supergravity with $A_0 = 0$, $\tan\beta = 10$, and $\mu > 0$. The excluded green regions are as in Fig. 6. The blue (yellow) shaded region has $0.1 < \Omega_{\rm DM}h^2 < 0.3$ ($0.025 < \Omega_{\rm DM}h^2 < 1$). The regions probed extend the curves toward the excluded green regions. From [95]. (For interpretation of the references to color in this figure legend, the reader is referred to the web version of this paper.)

Table 4
Constraints on supersymmetric models used in Fig. 19

Observable	Type	Bound	Experiment(s)
$\tilde{\chi}^\pm\tilde{\chi}^0$	Collider	See [96–98]	Tevatron Run II
$B \to X_s\gamma$	Low energy	$\lvert\Delta B(B \to X_s\gamma)\rvert < 1.2 \times 10^{-4}$	BaBar, BELLE
Muon MDM	Low energy	$\lvert a_\mu^{\rm SUSY}\rvert < 8 \times 10^{-10}$	Brookhaven E821
$\sigma_{\rm proton}$	Direct DM	Fig. 13	CDMS2, CRESST2
ν from Earth	Indirect DM	$\Phi_\mu^\oplus < 100\ \ {\rm km}^{-2}\ {\rm yr}^{-1}$	AMANDA
ν from Sun	Indirect DM	$\Phi_\mu^\odot < 100\ \ {\rm km}^{-2}\ {\rm yr}^{-1}$	AMANDA
γ (gal. center)	Indirect DM	$\Phi_\gamma(1) < 1.5 \times 10^{-10}\ {\rm cm}^{-2}\ {\rm s}^{-1}$	GLAST
γ (gal. center)	Indirect DM	$\Phi_\gamma(50) < 7 \times 10^{-12}\ {\rm cm}^{-2}\ {\rm s}^{-1}$	HESS, MAGIC
e^+ cosmic rays	Indirect DM	$(S/B)_{\rm max} < 0.01$	AMS-02

We also list experiments likely to reach these sensitivities in the near future. From [95].

sis (BBN), the cosmic microwave background, inflation, and reheating. Gravitino cosmology is in many ways complementary to neutralino cosmology, providing another rich arena for connections between microscopic physics and cosmology.

4.1. Gravitino properties

The properties of gravitinos may be systematically derived by supersymmetrizing the standard model coupled to gravity. Here, we will be content with highlighting the main results.

In an exactly supersymmetric theory, the gravitino is a massless spin 3/2 particle with two degrees of freedom. Once supersymmetry is broken, the gravitino eats a spin 1/2 fermion, the Goldstino of supersymmetry breaking, and becomes a massive spin 3/2 particle with four degrees of freedom. As noted in Section 2.5, the resulting gravitino mass is

$$m_{\tilde{G}} = \frac{F}{\sqrt{3}M_*}, \tag{37}$$

where $M_* \equiv (8\pi G_N)^{-1/2} \simeq 2.4 \times 10^{18}$ GeV is the reduced Planck mass. Gravitinos couple standard model particles to their superpartners through gravitino-gaugino-gauge boson interactions

$$L = -\frac{\mathrm{i}}{8M_*}\bar{\tilde{G}}_\mu[\gamma^\nu, \gamma^\rho]\gamma^\mu \tilde{V} F_{\nu\rho}, \tag{38}$$

and gravitino–sfermion–fermion interactions

$$L = -\frac{1}{\sqrt{2}M_*}\partial_\nu \tilde{f}\bar{f}\,\gamma^\mu\gamma^\nu\tilde{G}_\mu. \tag{39}$$

In models with high-scale supersymmetry breaking, such as conventional supergravity theories, $F \sim M_{\mathrm{weak}}M_*$, as explained in Section 2.5. The gravitino mass is therefore of the order of the other superpartner masses, and we expect them all to be in the range $\sim$100 GeV – 1 TeV. The gravitino's effective couplings are $\sim E/M_*$, where E is the energy of the process. The gravitino's interactions are therefore typically extremely weak, as they are suppressed by the Planck scale.

We will focus on theories with high-scale supersymmetry breaking in the following discussion. Note, however, that in theories with low-scale supersymmetry breaking, the gravitino may be much lighter, for example, as light as $\sim$eV in some simple gauge-mediated supersymmetry breaking models. The gravitino's interactions through its Goldstino components may also be much stronger, suppressed by F/M_{weak} rather than M_*. For a summary of gravitino cosmology in such scenarios, see [99].

4.2. Thermal relic density

If gravitinos are to play a cosmological role, we must first identify their production mechanism. There are a number of possibilities. Given our discussion of the neutralino thermal relic density in Section 3, a natural starting place is to consider gravitino production as a result of freeze out from thermal equilibrium. At present, the gravitino coupling E/M_* is a huge suppression. However, if we extrapolate back to very early times with temperatures $T \sim M_*$, even gravitational couplings were strong, and gravitinos were in thermal equilibrium, with $n_{\tilde{G}} = n_{\mathrm{eq}}$. Once the temperature drops below the Planck scale, however, gravitinos quickly decouple with the number density appropriate for relativistic particles. Following decoupling, their number density then satisfies $n_{\tilde{G}} \propto R^{-3} \propto T^3$. This has the same scaling behavior as

the background photon number density, however, and so we expect roughly similar number densities now.

If such gravitinos are stable, they could be dark matter. In fact, the first supersymmetric dark matter candidate proposed was the gravitino [100]. However, the overclosure bound implies

$$\Omega_{\tilde{G}} \lesssim 1 \Rightarrow m_{\tilde{G}} \lesssim 1 \text{ keV}. \tag{40}$$

This is not surprising—relic neutrinos have a similar density, and the overclosure bound on their mass is similar.

On the other hand, gravitinos may be unstable [101]. This may be because R-parity is broken, or because the gravitino is not the LSP. In this case, there is no bound from overclosure, but there are still constraints. In particular, the gravitino's decay products will destroy the successful predictions of BBN for light element abundances if the decay takes place after BBN. In the case where decay to a lighter supersymmetric particle is possible, we can estimate the gravitino lifetime to be

$$\tau_{\tilde{G}} \sim \frac{M_*^2}{m_{\tilde{G}}^3} \sim 0.1 \text{ yr} \left[\frac{100 \text{ GeV}}{m_{\tilde{G}}}\right]^3. \tag{41}$$

Requiring gravitino decays to be completed before BBN at $t \sim 1$ s implies [101]

$$m_{\tilde{G}} \gtrsim 10 \text{ TeV}. \tag{42}$$

In both cases, the required masses are incompatible with the most natural expectations of conventional supergravity theories. Gravitinos may, however, be a significant component of dark matter if they are stable with mass ~keV. Such masses are possible in low-scale supersymmetry breaking scenarios, given an appropriately chosen supersymmetry-breaking scale F.

4.3. Production during reheating

In the context of inflation, the gravitino production scenario of Section 4.2 is rather unnatural. Between the time when $T \sim M_*$ and now, we expect the universe to inflate, which would dilute any gravitino relic thermal density. Inflation does provide another source for gravitinos, however. Specifically, following inflation, we expect an era of reheating, during which the energy of the inflaton potential is transferred to standard model particles and superpartners, creating a hot thermal bath in which gravitinos may be produced [102–106].

After reheating, the universe is characterized by three hierarchically separated rates: the interaction rate of standard model particles and their superpartners with each other, $\sigma_{\text{SM}} n$; the expansion rate, H; and the rate of interactions involving one gravitino, $\sigma_{\tilde{G}} n$. Here n is the number density of standard model particles. After reheating, the universe is expected to have a temperature well below the Planck scale, but still well above standard model masses. These rates may then be estimated by dimensional analysis, and we find

$$\sigma_{\text{SM}} n \sim T \gg H \sim \frac{T^2}{M_*} \gg \sigma_{\tilde{G}} n \sim \frac{T^3}{M_*^2}. \tag{43}$$

The picture that emerges, then, is that after reheating, there is a thermal bath of standard model particles and their superpartners. Occasionally these interact to produce a gravitino through interactions like $gg \to \tilde{g}\tilde{G}$. The produced gravitinos then propagate through the universe essentially without interacting. If they are stable, as we will assume throughout this section, they contribute to the present dark matter density.

To determine the gravitino abundance, we turn once again to the Boltzmann equation

$$\frac{\mathrm{d}n}{\mathrm{d}t} = -3Hn - \langle \sigma_{\mathrm{A}} v \rangle (n^2 - n_{\mathrm{eq}}^2). \tag{44}$$

In this case, the source term n_{eq}^2 arises from interactions such as $gg \to \tilde{g}\tilde{G}$. In contrast to our previous application of the Boltzmann equation in Section 3.1, however, here the n^2 sink term, originating from interactions such as $\tilde{g}\tilde{G} \to gg$, is negligible. Changing variables as before with $t \to T$ and $n \to Y \equiv n/s$, we find

$$\frac{\mathrm{d}Y}{\mathrm{d}T} = -\frac{\langle \sigma_{\tilde{G}} v \rangle}{HTs} n^2. \tag{45}$$

The right-hand side is independent of T, since $n \propto T^3$, $H \propto T^2$ and $s \propto T^3$. We thus find an extremely simple relation—the gravitino relic number density is linearly proportional to the reheat temperature T_{R}.

The constant of proportionality is the gravitino production cross-section. The leading $2 \to 2$ QCD interactions have been included in [107]. These are listed in Fig. 20. With these results, the gravitino relic density can be determined as a function

	process i	$\lvert\mathcal{M}_i\rvert^2 / \frac{g^2}{M^2}\left(1 + \frac{m_{\tilde{g}}^2}{3m_{\tilde{G}}^2}\right)$
A	$g^a + g^b \to \tilde{g}^c + \tilde{G}$	$4(s + 2t + 2\frac{t^2}{s})\lvert f^{abc}\rvert^2$
B	$g^a + \tilde{g}^b \to g^c + \tilde{G}$	$-4(t + 2s + 2\frac{s^2}{t})\lvert f^{abc}\rvert^2$
C	$\tilde{q}_i + g^a \to q_j + \tilde{G}$	$2s\lvert T_{ji}^a\rvert^2$
D	$g^a + q_i \to \tilde{q}_j + \tilde{G}$	$-2t\lvert T_{ji}^a\rvert^2$
E	$\bar{\tilde{q}}_i + q_j \to g^a + \tilde{G}$	$-2t\lvert T_{ji}^a\rvert^2$
F	$\tilde{g}^a + \tilde{g}^b \to \tilde{g}^c + \tilde{G}$	$-8\frac{(s^2+st+t^2)^2}{st(s+t)}\lvert f^{abc}\rvert^2$
G	$q_i + \tilde{g}^a \to q_j + \tilde{G}$	$-4(s + \frac{s^2}{t})\lvert T_{ji}^a\rvert^2$
H	$\tilde{q}_i + \tilde{g}^a \to \tilde{q}_j + \tilde{G}$	$-2(t + 2s + 2\frac{s^2}{t})\lvert T_{ji}^a\rvert^2$
I	$q_i + \bar{q}_j \to \tilde{g}^a + \tilde{G}$	$-4(t + \frac{t^2}{s})\lvert T_{ji}^a\rvert^2$
J	$\tilde{q}_i + \bar{\tilde{q}}_j \to \tilde{g}^a + \tilde{G}$	$2(s + 2t + 2\frac{t^2}{s})\lvert T_{ji}^a\rvert^2$

Fig. 20. Processes contributing to gravitino production after reheating. From [107].

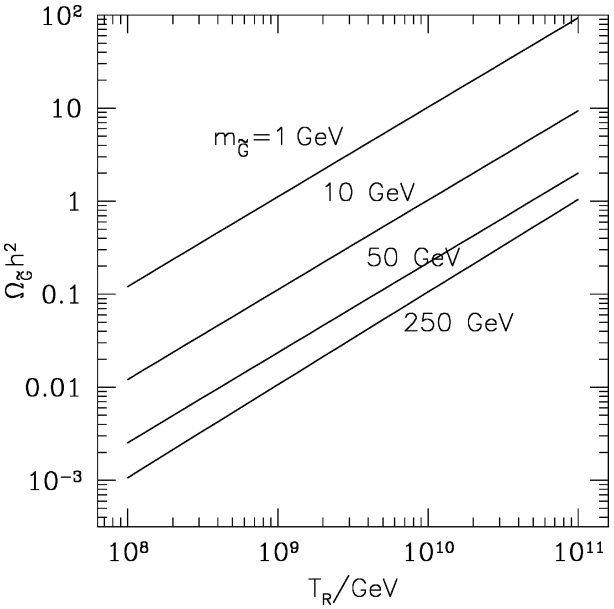

Fig. 21. The gravitino relic abundance $\Omega_{\tilde{G}}h^2$ as a function of reheating temperature T_R for various gravitino masses and gluino mass $m_{\tilde{g}} = 700$ GeV. From [107].

of reheating temperature T_R and gravitino mass. The results are given in Fig. 21. For gravitino mass $m_{\tilde{G}} \sim 100$ GeV, the constraint on $\Omega_{\rm DM}$ requires reheating temperature $T_R \lesssim 10^{10}$ GeV, providing a bound on the inflaton potential. Of course, if this bound is nearly saturated, gravitinos produced after reheating may be a significant component of dark matter.

4.4. Production from late decays

A third mechanism for gravitino production is through the cascade decays of other supersymmetric particles. If the gravitino is not the LSP, cascade decays will bypass the gravitino, given its highly suppressed couplings. However, as discussed in Section 2.5, the gravitino may be the LSP, even in high-scale supersymmetry breaking models. If the gravitino is the LSP, all cascades will ultimately end in a gravitino.

An alternative gravitino dark matter scenario is therefore the following [108,109]. Assume that the gravitino is the LSP and stable. To separate this scenario from the previous two, assume that inflation dilutes the primordial gravitino density and the universe reheats to a temperature low enough that gravitino production is negligible. Because the gravitino couples only gravitationally with all interactions suppressed by the Planck scale, it plays no role in the thermodynamics of the early universe. The next-to-lightest supersymmetric particle (NLSP) therefore freezes out as usual; if it is weakly interacting, its relic density will be near the desired value. However, much later, after

$$\tau \sim \frac{M_*^2}{M_{\rm weak}^3} \sim 10^5\text{–}10^8 \text{ s}, \tag{46}$$

the NLSP decays to the gravitino LSP. The gravitino therefore becomes dark matter with relic density

$$\Omega_{\tilde{G}} = \frac{m_{\tilde{G}}}{m_{\rm NLSP}} \Omega_{\rm NLSP}. \tag{47}$$

The gravitino and NLSP masses are naturally of the same order in theories with high-scale supersymmetry breaking. Gravitino LSPs may therefore form a significant relic component of our universe, inheriting the desired relic density from WIMP decay. In contrast to the previous two production mechanisms, the desired relic density is achieved naturally without the introduction of new energy scales.

Given our discussion in Section 4.2, the decay time of Eq. (46), well after BBN, should be of concern. In the present case, the decaying particle is a WIMP and so has a density far below that of a relativistic particle. (Recall Fig. 7.) However, one must check to see if the light element abundances are greatly perturbed. In fact, for some weak-scale NLSP and gravitino masses they are, and for some they are not [108,109]. We discuss this below, along with other constraints on this scenario.

Models with weak-scale extra dimensions also provide a similar dark matter particle in the form of Kaluza-Klein gravitons [108,114], with Kaluza-Klein gauge bosons or leptons playing the role of the decaying WIMP [58,59]. Because such dark matter candidates naturally preserve the WIMP relic abundance, but have interactions that are weaker than weak, they have been named superweakly interacting massive particles, or "superWIMPs."[3]

We see now that our discussion in Section 3 of WIMP dark matter was only valid for the "half" of parameter space where $m_{3/2} > m_{\rm LSP}$. When the gravitino is the LSP, there are number of new implications of supersymmetry for cosmology. For example, the "$\tilde{\tau}$ LSP" region is no longer excluded by searches for charged dark matter [108,109,115,116], as the $\tilde{\tau}$ is no longer stable, but only metastable. There is therefore the possibility of stable heavy charged particles appearing in collider detectors [117,118]. Further, regions with too much dark matter are no longer excluded, because the gravitino dark matter density is reduced by $m_{\tilde{G}}/m_{\rm NLSP}$ relative to the NLSP density. As we will discuss below, the late decays producing gravitinos may have detectable consequences for BBN and the cosmic microwave background. Astrophysical signatures in the diffuse photon spectrum [108], the ionization of the universe [119], and the suppression of small scale structure [120] are also interesting possibilities.

4.5. Detection

If gravitinos are the dark matter, all direct and indirect searches for dark matter are hopeless, because all interaction cross sections and annihilation rates are suppressed by the Planck scale. Instead, one must turn to finding evidence for gravitino

[3] A different dark matter candidate that also predicts late decays is axinos [110–113].

production in the early universe. In the case of gravitinos produced at $T \sim M_*$ or during reheating, the relevant physics is at such high energy scales that signals are absent, or at least require strong theoretical assumptions. In the case of production by late decays, however, there are several possible early universe signals. We consider a few of these in this section.

4.5.1. Energy release

If gravitinos are produced by late decays, the relevant reaction is NLSP $\to \tilde{G} + S$, where S denotes one or more standard model particles. Because the gravitino is essentially invisible, the observable consequences rely on finding signals of S production in the early universe. Signals from late decays have been considered in [121–131]. In principle, the strength of these signals depends on what S is and its initial energy distribution. It turns out, however, that most signals depend only on the time of energy release, that is, the NLSP's lifetime τ, and the average total electromagnetic or hadronic energy released in NLSP decay.

Here we will consider two possible NLSPs: the photino and the stau. In the photino case,

$$\Gamma(\tilde{\gamma} \to \gamma \tilde{G}) = \frac{1}{48\pi M_*^2} \frac{m_{\tilde{\gamma}}^5}{m_{\tilde{G}}^2} \left[1 - \frac{m_{\tilde{G}}^2}{m_{\tilde{\gamma}}^2}\right]^3 \left[1 + 3\frac{m_{\tilde{G}}^2}{m_{\tilde{\gamma}}^2}\right]. \tag{48}$$

In the limit $\Delta m \equiv m_{\tilde{\gamma}} - m_{\tilde{G}} \ll m_{\tilde{G}}$, the decay lifetime is

$$\tau(\tilde{\gamma} \to \gamma \tilde{G}) \approx 1.8 \times 10^7 \text{ s} \left[\frac{100 \text{ GeV}}{\Delta m}\right]^3, \tag{49}$$

independent of the overall superpartner mass scale. For the stau case,

$$\Gamma(\tilde{\tau} \to \tau \tilde{G}) = \frac{1}{48\pi M_*^2} \frac{m_{\tilde{\tau}}^5}{m_{\tilde{G}}^2} \left[1 - \frac{m_{\tilde{G}}^2}{m_{\tilde{\tau}}^2}\right]^4. \tag{50}$$

In the limit $\Delta m \equiv m_{\tilde{\tau}} - m_{\tilde{G}} \ll m_{\tilde{G}}$, the decay lifetime is

$$\tau(\tilde{\tau} \to \tau \tilde{G}) \approx 3.6 \times 10^8 \text{ s} \left[\frac{100 \text{ GeV}}{\Delta m}\right]^4 \frac{m_{\tilde{G}}}{1 \text{ TeV}}. \tag{51}$$

The electromagnetic energy release is conveniently written in terms of

$$\zeta_{\text{EM}} \equiv \varepsilon_{\text{EM}} Y_{\text{NLSP}}, \tag{52}$$

where ε_{EM} is the initial electromagnetic energy released in each NLSP decay, and $Y_{\text{NLSP}} \equiv n_{\text{NLSP}}/n_\gamma^{\text{BG}}$ is the NLSP number density before they decay, normalized to the number density of background photons $n_\gamma^{\text{BG}} = 2\zeta(3)T^3/\pi^2$. We define hadronic energy release similarly as $\zeta_{\text{had}} \equiv \varepsilon_{\text{had}} Y_{\text{NLSP}}$.

NLSP velocities are negligible when they decay, and so the potentially visible energy is

$$E_S \equiv \frac{m_{\text{NLSP}}^2 - m_{\tilde{G}}^2}{2m_{\text{NLSP}}}. \tag{53}$$

For the photino case, $S = \gamma$. At leading order, all of the initial photon energy is deposited in an electromagnetic shower, and so

$$\varepsilon_{\rm EM} = E_\gamma, \quad \varepsilon_{\rm had} \simeq 0. \tag{54}$$

For the stau case,

$$\varepsilon_{\rm EM} \approx \tfrac{1}{3}E_\tau - E_\tau, \quad \varepsilon_{\rm had} = 0, \tag{55}$$

where the range in $\varepsilon_{\rm EM}$ results from the possible variation in electromagnetic energy from $\pi^\pm$ and ν decay products. The precise value of $\varepsilon_{\rm EM}$ is in principle calculable once the stau's chirality and mass, and the superWIMP mass, are specified. However, as the possible variation in $\varepsilon_{\rm EM}$ is not great relative to other effects, we will simply present results below for the representative value of $\varepsilon_{\rm EM} = \frac{1}{2}E_\tau$.

The lifetimes and energy releases in the photino and stau NLSP scenarios are given in Fig. 22 for a range of $(m_{\rm NLSP}, \Delta m)$. For natural weak-scale values of these parameters, the lifetimes and energy releases in the neutralino and stau scenarios are similar, with lifetimes of about a year, in accord with the rough estimate of Eq. (46), and energy releases of

$$\zeta_{\rm EM} \sim 10^{-9}\ {\rm GeV}. \tag{56}$$

Such values have testable implications, as we now discuss.

4.5.2. Big Bang nucleosynthesis

Big Bang nucleosynthesis predicts primordial light element abundances in terms of one free parameter, the baryon-to-photon ratio $\eta \equiv n_B/n_\gamma$. At present, the observed

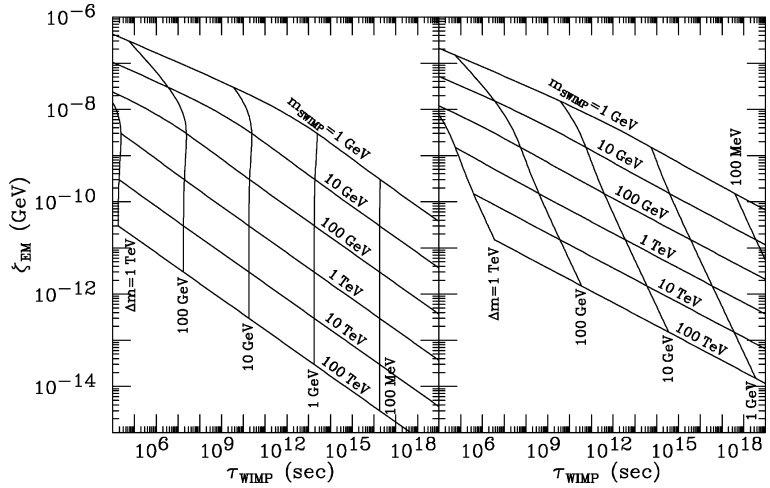

Fig. 22. Predicted values of NLSP lifetime τ and electromagnetic energy release $\zeta_{\rm EM} \equiv \varepsilon_{\rm EM} Y_{\rm NLSP}$ in the $\tilde{\gamma}$ (left) and $\tilde{\tau}$ (right) NLSP scenarios for $m_{\tilde{G}} = 1\ {\rm GeV}, 10\ {\rm GeV}, \ldots, 100\ {\rm TeV}$ (top to bottom) and $\Delta m \equiv m_{\rm NLSP} - m_{\tilde{G}} = 1\ {\rm TeV}, 100\ {\rm GeV}, \ldots, 100\ {\rm MeV}$ (left to right). For the $\tilde{\tau}$ NLSP scenario, we assume $\varepsilon_{\rm EM} = \frac{1}{2}E_\tau$. From [109].

D, ^{4}He, ^{3}He, and ^{7}Li abundances may be accommodated for baryon-to-photon ratios in the range [132]

$$\eta_{10} \equiv \eta/10^{-10} = 2.6\text{–}6.2. \tag{57}$$

(see Fig. 23.) In light of the difficulty of making precise theoretical predictions and reducing (or even estimating) systematic uncertainties in the observations, this consistency is a well-known triumph of standard Big Bang cosmology.

At the same time, given recent and expected advances in precision cosmology, the standard BBN picture merits close scrutiny. Recently, BBN baryometry has been supplemented by CMB data, which alone yields $\eta_{10} = 6.1 \pm 0.4$ [1]. Observations of deuterium absorption features in spectra from high redshift quasars imply a primordial D fraction of $\mathrm{D/H} = 2.78^{+0.44}_{-0.38} \times 10^{-5}$ [134]. Combined with standard BBN calculations [135], this yields $\eta_{10} = 5.9 \pm 0.5$. The remarkable agreement between CMB and D baryometers has two new implications for scenarios with late-decaying particles. First, assuming there is no fine-tuned cancellation of unrelated effects, it prohibits significant entropy production between the times of BBN and decoupling. Second, the CMB measurement supports determinations of η from D, already considered by many to be the most reliable BBN baryometer. It suggests that if D and another BBN baryometer disagree, the "problem" lies with the other light element abundance—either its systematic uncertainties have been underestimated, or its value is modified by new astrophysics or particle physics. At present BBN predicts a ^{7}Li abundance significantly greater observed. This disagreement may therefore provide specific evidence for late-decaying particles in general, and gravitino dark matter in particular.

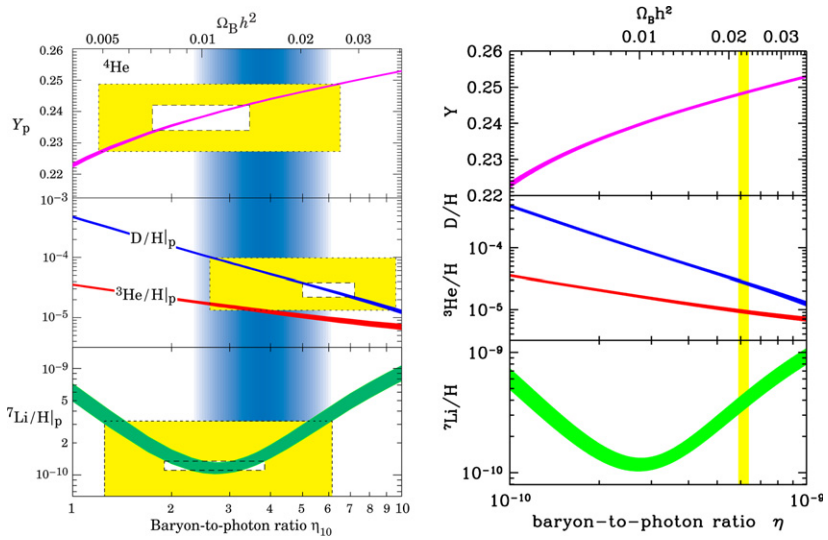

Fig. 23. Bounds on the baryon density $\Omega_B h^2$ from BBN (left, from [132]) and the CMB (right, from [133]). The new and extremely precise CMB constraint favors the BBN $\Omega_B h^2$ determination from deuterium and implies that the ^{7}Li abundance is anomalously low.

Given the overall success of BBN, the first implication for new physics is that it should not drastically alter any of the light element abundances. This requirement restricts the amount of energy released at various times in the history of the universe. A recent analysis of electromagnetic cascades finds that the shaded regions of Fig. 24 are excluded by such considerations [127]. The various regions are disfavored by the following conservative criteria:

$$\text{D low}: \quad \mathrm{D/H} < 1.3 \times 10^{-5}, \tag{58}$$

$$\text{D high}: \quad \mathrm{D/H} > 5.3 \times 10^{-5}, \tag{59}$$

$$^4\text{He low}: \quad Y_p < 0.227, \tag{60}$$

$$^7\text{Li low}: \quad {}^7\mathrm{Li/H} < 0.9 \times 10^{-10}. \tag{61}$$

A subset of superWIMP predictions from Fig. 22 is superimposed on this plot. The subset is for weak-scale $m_{\tilde{G}}$ and Δm, the most natural values, given the independent motivations for new physics at the weak scale. The BBN constraint eliminates some of the region predicted by the superWIMP scenario, but regions with m_{NLSP}, $m_{\tilde{G}} \sim M_{\mathrm{weak}}$ remain viable.

The ^{7}Li anomaly discussed above may be taken as evidence for new physics, however. To improve the agreement of observations and BBN predictions, it is necessary to destroy ^{7}Li without harming the concordance between CMB and other BBN deter-

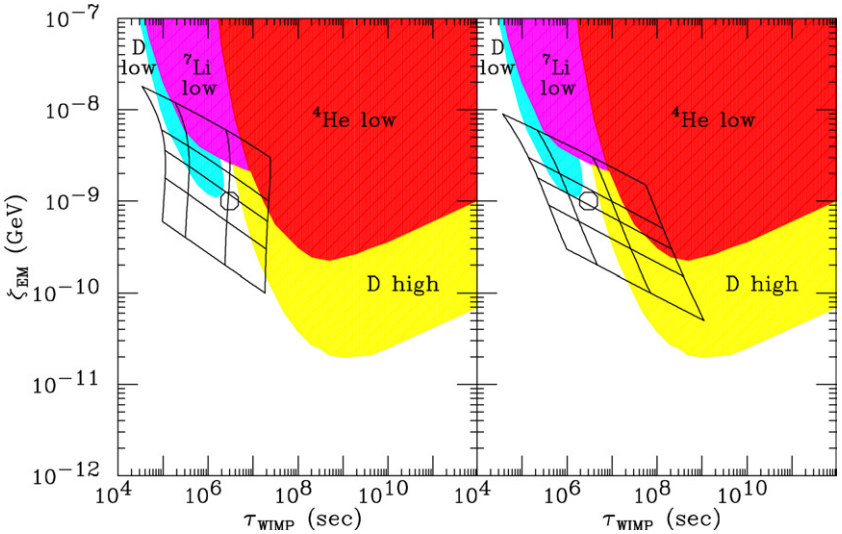

Fig. 24. The grid gives predicted values of NLSP lifetime τ and electromagnetic energy release $\zeta_{\mathrm{EM}} \equiv \varepsilon_{\mathrm{EM}} Y_{\mathrm{NLSP}}$ in the $\tilde{\gamma}$ (left) and $\tilde{\tau}$ (right) NLSP scenarios for $m_{\tilde{G}} = 100, 300,$ and 500 GeV, 1 TeV, and 3 TeV (top to bottom) and $\Delta m \equiv m_{\mathrm{NLSP}} - m_{\tilde{G}} = 600, 400, 200,$ and 100 GeV (left to right). For the $\tilde{\tau}$ NLSP scenario, we assume $\varepsilon_{\mathrm{EM}} = \frac{1}{2} E_\tau$. BBN constraints exclude the shaded regions [127]. The best fit region with $(\tau, \zeta_{\mathrm{EM}}) \sim (3 \times 10^6\ \mathrm{s}, 10^{-9}\ \mathrm{GeV})$, where ^{7}Li is reduced to observed levels by late decays of NLSPs to gravitinos, is given by the circle. From [109].

minations of η. This may be accomplished for $(\tau,\zeta_{\rm EM}) \sim (3\times 10^6\ {\rm s}, 10^{-9}\ {\rm GeV})$ [127]. This "best fit" point is marked in Fig. 24. The amount of energy release is determined by the requirement that ^{7}Li be reduced to observed levels without being completely destroyed—one cannot therefore be too far from the "^{7}Li low" region. In addition, one cannot destroy or create too much of the other elements. ^{4}He, with a binding threshold energy of 19.8 MeV, much higher than Lithium's 2.5 MeV, is not significantly destroyed. On the other hand, D is loosely bound, with a binding energy of 2.2 MeV. The two primary reactions are D destruction through $\gamma{\rm D}\to {\rm np}$ and D creation through $\gamma\,{}^4{\rm He}\to {\rm DD}$. These are balanced in the channel of Fig. 24 between the "low D" and "high D" regions, and the requirement that the electromagnetic energy that destroys ^{7}Li not disturb the D abundance specifies the preferred decay time $\tau\sim 3\times 10^6$ s.

Without theoretical guidance, this scenario for resolving the ^{7}Li abundance is rather fine-tuned: possible decay times and energy releases span tens of orders of magnitude, and there is no motivation for the specific range of parameters required to resolve BBN discrepancies. In the superWIMP scenario, however, both τ and $\zeta_{\rm EM}$ are specified: the decay time is necessarily that of a gravitational decay of a weak-scale mass particle, leading to Eq. (46), and the energy release is determined by the requirement that superWIMPs be the dark matter, leading to Eq. (56). Remarkably, these values coincide with the best fit values for τ and $\zeta_{\rm EM}$. More quantitatively, we note that the grids of predictions for the $\tilde\gamma$ and $\tilde\tau$ scenarios given in Fig. 24 cover the best fit region. Current discrepancies in BBN light element abundances may therefore be naturally explained by gravitino dark matter.

This tentative evidence may be reinforced or disfavored in a number of ways. Improvements in the BBN observations discussed above may show if the ^{7}Li abundance is truly below predictions. In addition, measurements of ^{6}Li/H and ^{6}Li/^{7}Li may constrain astrophysical depletion of ^{7}Li and may also provide additional evidence for late decaying particles in the best fit region [124,136,125,127,137]. Finally, if the best fit region is indeed realized by NLSP $\to \tilde G$ decays, there are a number of other testable implications for cosmology and particle physics. We discuss one of these in the following section. Additional discussion, including diffuse photon signals, the implications of hadronic energy release, and novel collider analyses, may be found in [108,109,138–143].

4.5.3. The cosmic microwave background

The injection of electromagnetic energy may also distort the frequency dependence of the CMB black body radiation. For the decay times of interest, with redshifts $z\sim 10^5$–10^7, the resulting photons interact efficiently through $\gamma e^-\to\gamma e^-$, but photon number is conserved, since double Compton scattering $\gamma e^-\to\gamma\gamma e^-$ and thermal bremsstrahlung $eX\to eX\gamma$, where X is an ion, are inefficient. The spectrum therefore relaxes to statistical but not thermodynamic equilibrium, resulting in a Bose-Einstein distribution function

$$f_\gamma(E) = \frac{1}{{\rm e}^{E/(kT)+\mu}-1}, \tag{62}$$

with chemical potential $\mu\neq 0$.

For the low values of baryon density currently favored, the effects of double Compton scattering are more significant than those of thermal bremsstrahlung. The value of the chemical potential μ may therefore be approximated for small energy releases by the analytic expression [144]

$$\mu = 8.0 \times 10^{-4} \left[\frac{\tau}{10^6 \text{ s}}\right]^{1/2} \left[\frac{\zeta_{\text{EM}}}{10^{-9} \text{ GeV}}\right] e^{-(\tau_{\text{dC}}/\tau)^{5/4}}, \tag{63}$$

where

$$\tau_{\text{dC}} = 6.1 \times 10^6 \text{ s} \left[\frac{T_0}{2.725 \text{ K}}\right]^{-12/5} \left[\frac{\Omega_{\text{B}} h^2}{0.022}\right]^{4/5} \left[\frac{1 - \frac{1}{2} Y_p}{0.88}\right]^{4/5}. \tag{64}$$

In Fig. 25 we show contours of chemical potential μ. The current bound is $\mu < 9 \times 10^{-5}$ [145,132]. We see that, although there are at present no indications of deviations from black body, current limits are already sensitive to the superWIMP scenario, and particularly to regions favored by the BBN considerations described in Section 4.5.2. In the future, the Diffuse Microwave Emission Survey (DIMES) may improve sensitivities to $\mu \approx 2 \times 10^{-6}$ [146]. DIMES will therefore probe further into superWIMP parameter space, and will effectively probe all of the favored region where the ^{7}Li underabundance is explained by gravitino dark matter.

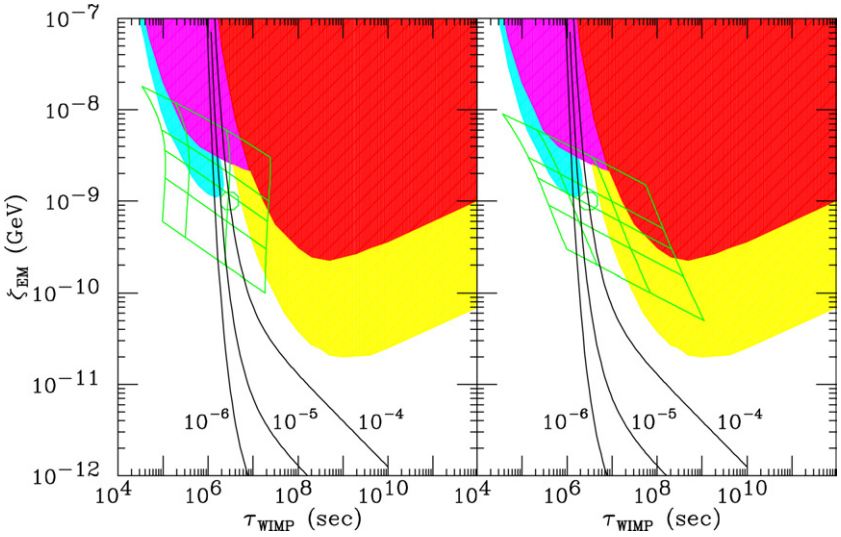

Fig. 25. Contours of μ, parameterizing the distortion of the CMB from a Planckian spectrum, in the $(\tau, \zeta_{\text{EM}})$ plane. Regions predicted by the gravitino dark matter scenario, and BBN excluded and best fit regions are given as in Fig. 24. From [109].

4.6. Summary

- The gravitino mass is determined by the scale of supersymmetry breaking and may be anywhere in the range from eV to TeV. In supergravity theories, its mass is at the weak scale and its couplings are suppressed by the Planck scale, and so extremely weak.
- If gravitinos are produced as a thermal relic, their mass is bounded by overclosure to be $m_{\tilde{G}} \lesssim$ keV if they are stable, and by BBN to be $m_{\tilde{G}} \gtrsim 10$ TeV if they are unstable.
- Gravitinos may be produced after inflation during reheating. For stable weak-scale gravitinos, overclosure places an upper bound on the reheat temperature of the order of 10^{10} GeV.
- Weak-scale gravitinos may also be produced in NLSP decays at time $t \sim 10^4$–10^8 s. In this case, gravitinos may be dark matter, naturally inheriting the desired relic density. Gravitino dark matter is undetectable by conventional direct and indirect dark matter searches, but may be discovered through its imprint on early universe signals, such as BBN and the CMB.

5. Prospects

We have now discussed a wide variety of cosmological implications of supersymmetry. If discoveries are made in astrophysical and cosmological observations, what are the prospects for determining if this new physics is supersymmetry? Put more generally, what are the prospects for a microscopic understanding of the dark universe? Such questions are grand, and their answers speculative. Nevertheless, some lessons may be drawn even now. As we will see, even in the best of cases, we will need diverse experiments from both particle physics and cosmology to explore this frontier.

5.1. The particle physics/cosmology interface

As a case study, let us confine our discussion to one topic: neutralino dark matter. We assume that non-baryonic dark matter is in fact neutralinos. If this is so, what are the prospects for establishing this, and what tools will we need?

It is first important to recognize the limitations of both cosmology and particle physics when taken separately:

- *Cosmological observations and astrophysical experiments cannot discover supersymmetry.* As noted in Section 1, cosmological data leaves the properties of dark matter largely unconstrained. If dark matter is discovered in direct or indirect detection experiments, its mass and interaction strengths will be bounded but only very roughly at first. (For example, the region favored by the DAMA signal spans factors of a few in both mass and interaction strength; see Fig. 14.) These con-

straints will be sharpened by follow-up experiments. However, the microscopic implications of such experiments are clouded by significant astrophysical ambiguities, such as the dark matter velocity distribution, halo profiles, etc. Even with signals in a variety of direct and indirect detection experiments, it is unlikely that dark matter properties will be constrained enough to differentiate supersymmetry from other reasonable possibilities.

- *Particle experiments cannot discover dark matter.* If weak-scale superpartners exist, particle colliders will almost certainly be able to discover at least some of them. However, even if they find all of them, the dark matter candidate will most likely appear only as missing energy and momentum. Furthermore, collider experiments can only test the stability of such particles up to lifetimes of $\sim 10^{-7}$ s. As we have seen in Section 4, lifetimes of a year or more are perfectly natural in well-motivated models of new physics. The conclusion that a particle seen in collider experiments is the dark matter therefore requires an unjustified extrapolation of 24 orders of magnitude in the particle's lifetime.

Through the combination of both approaches, however, it is possible that a cohesive and compelling theory of dark matter will emerge. A schematic picture of the combined investigation of neutralino dark matter is given in Fig. 26 [147]. Working from the bottom, cosmological observations have already determined the relic density with some precision. Future observations, such as by the Planck satellite [148], are likely to reduce uncertainties in the relic density determination to the 1% level, given now standard cosmological assumptions. Astrophysical experiments may also detect dark matter either directly through its interactions with ordinary matter or indirectly through its annihilation decay products. Such data, combined with astrophysical inputs such as the dark matter halo profile and local density, will provide information about the strength of χN scattering and $\chi\chi$ annihilation.

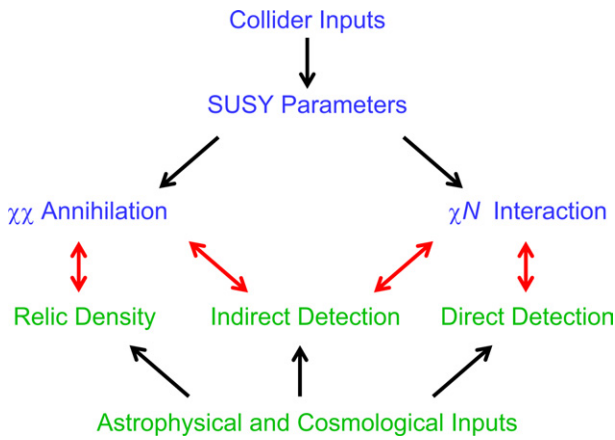

Fig. 26. The road to a microscopic understanding of neutralino dark matter.

At the same time, working from the top of Fig. 26, colliders will discover supersymmetry and begin to determine the parameters of the weak-scale Lagrangian. These parameters will, in principle, fix the neutralino's thermal relic density, the χN scattering cross-section, and the neutralino pair annihilation rates. Completion of this program at a high level of precision, followed by detailed comparison with the measured relic density and detection rates from cosmology and astrophysics will provide a great deal of information about the suitability of neutralinos as dark matter candidates.

5.2. The role of colliders

Clearly data from particle colliders will be required to identify neutralino dark matter. The requirements for colliders depend sensitively on what scenario is realized in nature. As examples, consider some of the cosmologically preferred regions of minimal supergravity discussed in Section 3.2. In the bulk region, one must verify that the neutralino is Bino-like and must determine the masses of sfermions that appear in the t-channel annihilation diagrams. In the focus point region, the neutralino's gauginoness must be precisely measured, whereas in the A funnel region, a high precision measurement of $m_A - 2m_\chi$ is critical. Finally, for the co-annihilation region, there is extreme sensitivity to the $\tilde{\tau} - \chi$ mass splitting. Measurements below the GeV level are required to accurately determine the predicted thermal relic density.

Let us consider the bulk region scenario in more detail. Not all sfermion masses need be measured. For example, if the right-handed sleptons are light, they typically give the dominant contribution, since these have the largest hypercharge Y and the annihilation diagram is proportional to Y^4. In such cases, measurements of $m_{\tilde{l}_R}$ and lower bounds on left-handed slepton and squark masses will provide a reasonable starting point.

The possibility of doing this at the LHC has been considered in [149]. In much of the bulk region, the cascade decay $\tilde{q}_L \to \tilde{\chi}_2^0 q \to \tilde{l}_R l q \to l^+ l^- \tilde{\chi}_1^0 q$ is open. Kinematic endpoints may then be used to determine the $\tilde{l}_R$ and $\tilde{\chi}_1^0$ masses precisely. Assuming that the lightest neutralino is Bino-like, one may then estimate the relic density, keeping only $\tilde{l}_R$ exchange diagrams. As shown in Fig. 27, this provides an estimate accurate to about $\sim$20% in minimal supergravity. Following this, one would then need to determine the gaugino-ness of the lightest neutralino and set lower bounds on the other sfermion masses.

At a linear collider, one may establish that the new particles being produced are supersymmetric by measuring their dimensionless couplings. One may then go on to determine the gaugino-ness of the LSP in a model-independent manner. For example, the cross-section $\sigma(e^+ e_R^- \to \tilde{\chi}^+ \tilde{\chi}^-)$ nearly vanishes for gaugino-like charginos. It therefore provides a sensitive measure of chargino gaugino-ness (see Fig. 28). Combined with kinematic measurements of the chargino mass, the parameters M_2 and μ may be measured precisely. Further measurements can use these results to pinpoint M_1 and $\tan\beta$, and thereby the gaugino-ness of the LSP. Precisions of $\sim$1% or better are possible, translating into predictions for relic densities and dark matter cross-sections that will match the precision expected from cosmological data.

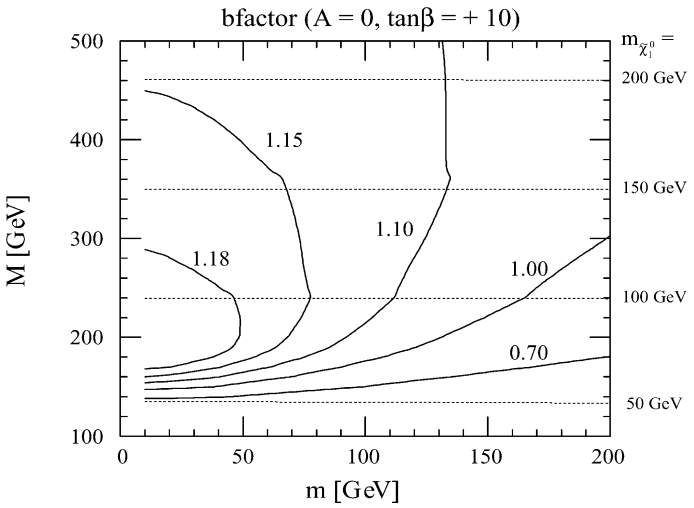

Fig. 27. The ratio of the true $\Omega_{\rm DM}h^2$ to that calculated with the $\tilde{l}_{\rm R}$ t-channel diagrams in the (m, M) plane, where m and M are the universal scalar and gaugino masses of minimal supergravity, respectively. From [149].

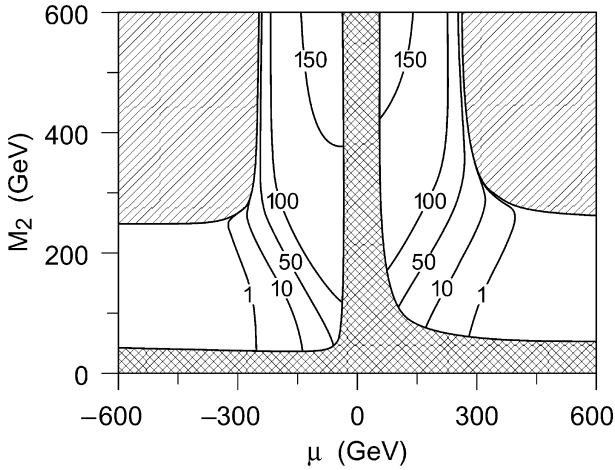

Fig. 28. Contours of constant cross-section $\sigma(e^+e_{\rm R}^- \to \tilde{\chi}^+\tilde{\chi}^-)$ for a $\sqrt{s} = 500$ GeV linear collider. From [150].

5.3. Synthesis

If the relic density and interaction strengths as determined by astrophysics and cosmology agree with the predictions of particle physics with high precision, this agreement will provide strong evidence that the dark matter is in fact supersymmetric. It will imply that we understand the history of the universe back to the freeze out

temperature ~10 GeV, or times $t \sim 10^{-8}$ s. Recall that our current knowledge of the history of the universe is on sure footing only back to Big Bang nucleosynthesis at temperatures of ~MeV, or times $t \sim 1$ s. Dark matter studies could therefore provide the necessary evidence to push back our knowledge of the universe another 8 orders of magnitude in time, a formidable achievement.

On the other hand, the determinations of relic density and dark matter interaction strengths by particle physics and cosmology may not agree. Progress then has many possible paths. If the disparity is great, one might look to other dark matter candidates, such as the axion [151–153] or other supersymmetric possibilities [154–156,110–112]. If the relic density determinations are reasonably close, one might explore the possibility that the neutralino is not stable, but deposits much of its relic density in a gravitino LSP, as discussed in Section 4.4.

Alternatively, one might look to non-standard cosmologies for a resolution. The identification of the thermal relic density with the present day cold dark matter density is subject to cosmological assumptions. The calculation of the thermal relic density assumes that the dominant source of dark matter is from dark matter particles falling out of thermal equilibrium. It is possible, however, that the bulk of the dark matter is created not through thermal equilibrium and freeze out, but through the out-of-equilibrium decay of a supermassive particle. The actual relic density would then be greater than the thermal relic density. The thermal relic density calculation also assumes that nothing unusual happens once the dark matter is produced at temperatures of $T \sim \mathcal{O}(10)$ GeV. Large entropy production by late-decaying particles may dilute calculated relic densities. In this case, the actual relic density would be less than the naive thermal relic density. The bottom line is that the cold dark matter density obtained following the path from the bottom of Fig. 26 need not coincide with the thermal relic density obtained by following the path from the top. Instead, discrepancies might provide new insights into the history of our universe.

In a similar vein, the neutralino–nucleon cross-sections need not match the dark matter detection rates. As stressed above, this correspondence requires astrophysical assumptions. The uncertainties and problems associated with these issues have been discussed extensively [28,29,31,32]. It is possible, however, that the relic densities, as determined independently by particle physics and cosmology, agree to 1%, but the detection rates differ. One would then be confident that neutralinos are the dark matter and particle physics uncertainties would be eliminated, allowing detection experiments to probe astrophysics. For example, direct detection rates would then provide information about the local dark matter density and velocity distributions, and indirect detection rates would provide information about halo profiles. The synergy between cosmology and particle physics would then truly come full circle.

5.4. Summary

A microscopic understanding of the dark universe is a challenging goal. As an example, we have focused here on prospects for a fundamental description of dark matter. Cosmological measurements, although able to bound total energy densities, cannot tell us much about the dark matter's microscopic properties. On the other

hand, particle physics experiments may produce dark matter and may measure its properties rather precisely, but cannot never establish its stability on cosmological time scales. It is only through the combination of approaches in particle physics, astrophysics, and cosmology that the identity of dark matter will be uncovered. The task requires many diverse experiments, and will likely take decades to complete. Nevertheless, if any of the connections between the weak scale and cosmology described here are realized in nature, one would be hard-pressed to envision a more exciting era of discovery than the coming years.

Acknowledgments

I am grateful to the organizers of the 2003 SLAC Summer Institute, where this material was first presented, and to the students and participants for their enthusiasm and lively discussions. I thank the many colleagues, especially Konstantin Matchev, Arvind Rajaraman, Fumihiro Takayama, and Frank Wilczek, who have helped to shape my understanding of the topics presented here. This work was supported in part by National Science Foundation CAREER Award PHY-0239817 and in part by the Alfred P. Sloan Foundation.

References

[1] D.N. Spergel et al., First year Wilkinson microwave anisotropy probe (WMAP) observations: determination of cosmological parameters. Available from: <astro-ph/0302209>.
[2] M. Tegmark et al. [SDSS Collaboration], Cosmological parameters from SDSS and WMAP. Available from: <astro-ph/0310723>.
[3] For proper introductions to supersymmetry, see, for example H.J. Muller-Kirsten, A. Wiedemann, Supersymmetry: An Introduction with Conceptual and Calculational Details, Print-86-0955 (KAISERSLAUTERN);
J. Wess, J. Bagger, Supersymmetry and Supergravity, second ed., Princeton University Press, Princeton, NJ, 1992;
H.E. Haber, Introductory low-energy supersymmetry. Available from: <hep-ph/9306207>;
X. Tata, Supersymmetry: where it is and how to find it. Available from: <hep-ph/9510287>;
M. Drees, An introduction to supersymmetry. Available from: <hep-ph/9611409>;
J.D. Lykken, Introduction to supersymmetry. Available from: <hep-th/9612114>;
S.P. Martin, A supersymmetry primer. Available from: <hep-ph/9709356>;
S. Weinberg, The Quantum Theory of Fields. Vol. 3: Supersymmetry, Cambridge University Press, Cambridge, UK, 2000;
N. Polonsky, Supersymmetry: Structure and Phenomena. Extensions of the Standard Model, Lect. Notes Phys. M 68 (2001) 1, Available from: <hep-ph/0108236>.
[4] R. Haag, J.T. Lopuszanski, M. Sohnius, Nucl. Phys. B 88 (1975) 257.
[5] S. Dimopoulos, S. Raby, F. Wilczek, Phys. Rev. D 24 (1981) 1681.
[6] A.H. Chamseddine, R. Arnowitt, P. Nath, Phys. Rev. Lett. 49 (1982) 970.
[7] R. Barbieri, S. Ferrara, C.A. Savoy, Phys. Lett. B 119 (1982) 343.
[8] N. Ohta, Prog. Theor. Phys. 70 (1983) 542.
[9] L.J. Hall, J. Lykken, S. Weinberg, Phys. Rev. D 27 (1983) 2359.
[10] L. Alvarez-Gaume, J. Polchinski, M.B. Wise, Nucl. Phys. B 221 (1983) 495.
[11] K.A. Olive, TASI lectures on dark matter. Available from: <astro-ph/0301505>.

[12] J.L. Feng, K.T. Matchev, F. Wilczek, Phys. Lett. B 482 (2000) 388, Available from: <hep-ph/0004043>.
[13] H. Goldberg, Phys. Rev. Lett. 50 (1983) 1419.
[14] J.R. Ellis, J.S. Hagelin, D.V. Nanopoulos, K.A. Olive, M. Srednicki, Nucl. Phys. B 238 (1984) 453.
[15] For proper introductions to dark matter, see, for example, [16,17,11] and L. Bergstrom, Rept. Prog. Phys. 63 (2000) 793. Available from: <hep-ph/0002126>.
[16] G. Jungman, M. Kamionkowski, K. Griest, Phys. Rept. 267 (1996) 195, Available from: <hep-ph/9506380>.
[17] E.W. Kolb, M.S. Turner, The Early Universe, Addison-Wesley, Redwood City, CA, 1990.
[18] M. Drees, M.M. Nojiri, Phys. Rev. D 47 (1993) 376, Available from: <hep-ph/9207234>.
[19] P. Gondolo, J. Edsjo, L. Bergstrom, P. Ullio, E.A. Baltz, DarkSUSY: A numerical package for dark matter calculations in the MSSM. Available from: <astro-ph/0012234>.
[20] J.R. Ellis, K.A. Olive, Y. Santoso, V.C. Spanos, Phys. Lett. B 565 (2003) 176, Available from: <hep-ph/0303043>.
[21] J.L. Feng, K.T. Matchev, T. Moroi, Phys. Rev. Lett. 84 (2000) 2322, Available from: <hep-ph/9908309>.
[22] J.L. Feng, K.T. Matchev, T. Moroi, Phys. Rev. D 61 (2000) 075005, Available from: <hep-ph/9909334>.
[23] J.L. Feng, K.T. Matchev, Phys. Rev. D 63 (2001) 095003, Available from: <hep-ph/0011356>.
[24] H. Baer, C. Balazs, A. Belyaev, JHEP 0203 (2002) 042, Available from: <hep-ph/0202076>.
[25] H. Baer, C. Balazs, A. Belyaev, Relic density of neutralinos in minimal supergravity. Available from: <hep-ph/0211213>.
[26] P. Binetruy, G. Girardi, P. Salati, Nucl. Phys. B 237 (1984) 285.
[27] K. Griest, D. Seckel, Phys. Rev. D 43 (1991) 3191.
[28] P. Sikivie, I.I. Tkachev, Y. Wang, Phys. Rev. D 56 (1997) 1863, Available from: <astro-ph/9609022>.
[29] M. Brhlik, L. Roszkowski, Phys. Lett. B 464 (1999) 303, Available from: <hep-ph/9903468>.
[30] P. Belli, R. Bernabei, A. Bottino, F. Donato, N. Fornengo, D. Prosperi, S. Scopel, Phys. Rev. D 61 (2000) 023512, Available from: <hep-ph/9903501>.
[31] G. Gelmini, P. Gondolo, Phys. Rev. D 64 (2001) 023504, Available from: <hep-ph/0012315>.
[32] C. Calcaneo-Roldan, B. Moore, Phys. Rev. D 62 (2000) 123005, Available from: <astro-ph/0010056>.
[33] M.W. Goodman, E. Witten, Phys. Rev. D 31 (1985) 3059.
[34] J.R. Ellis, A. Ferstl, K.A. Olive, Phys. Lett. B 481 (2000) 304, Available from: <hep-ph/0001005>.
[35] M.A. Shifman, A.I. Vainshtein, V.I. Zakharov, Phys. Lett. B 78 (1978) 443.
[36] H. Baer, C. Balazs, A. Belyaev, J. O'Farrill, JCAP 0309 (2003) 007, Available from: <hep-ph/0305191>.
[37] R. Bernabei et al. [DAMA Collaboration], Phys. Lett. B 480 (2000) 23.
[38] A. Benoit, et al., Phys. Lett. B 545 (2002) 43, Available from: <astro-ph/0206271>.
[39] D.S. Akerib et al. [CDMS Collaboration], Phys. Rev. D 68 (2003) 082002. Available from: <hep-ex/0306001>.
[40] D.S. Akerib et al. [CDMS Collaboration], First results from the cryogenic dark matter search in the Soudan underground lab. Available from: <astro-ph/0405033>.
[41] C.J. Copi, L.M. Krauss, Phys. Rev. D 67 (2003) 103507, Available from: <astro-ph/0208010>.
[42] K. Freese, P. Gondolo, H.J. Newberg, Detectability of weakly interacting massive particles in the Sagittarius dwarf tidal stream. Available from: <astro-ph/0309279>.
[43] P. Ullio, M. Kamionkowski, P. Vogel, JHEP 0107 (2001) 044, Available from: <hep-ph/0010036>.
[44] D.R. Smith, N. Weiner, Phys. Rev. D 64 (2001) 043502, Available from: <hep-ph/0101138>.
[45] A. Kurylov, M. Kamionkowski, Phys. Rev. D 69 (2004) 063503, Available from: <hep-ph/0307185>.
[46] D. Tucker-Smith, N. Weiner, The status of inelastic dark matter. Available from: <hep-ph/0402065>.
[47] S. Rudaz, F.W. Stecker, Astrophys. J. 325 (1988) 16.

[48] A.J. Tylka, Phys. Rev. Lett. 63 (1989) 840.
[49] M.S. Turner, F. Wilczek, Phys. Rev. D 42 (1990) 1001.
[50] M. Kamionkowski, M.S. Turner, Phys. Rev. D 43 (1991) 1774.
[51] E.A. Baltz, J. Edsjo, Phys. Rev. D 59 (1999) 023511, Available from: <astro-ph/9808243>.
[52] I.V. Moskalenko, A.W. Strong, Phys. Rev. D 60 (1999) 063003, Available from: <astro-ph/9905283>.
[53] F.W. Stecker, A.J. Tylka, Ap. J. 336 (1989) L51.
[54] P. Chardonnet, G. Mignola, P. Salati, R. Taillet, Phys. Lett. B 384 (1996) 161, Available from: <astro-ph/9606174>.
[55] L. Bergström, J. Edsjö, P. Ullio, Cosmic antiprotons as a probe for supersymmetric dark matter? Available from: <astro-ph/9902012>.
[56] J.W. Bieber, R.A. Burger, R. Engel, T.K. Gaisser, S. Roesler, T. Stanev, Phys. Rev. Lett. 83 (1999) 674, Available from: <astro-ph/9903163>.
[57] F. Donato, N. Fornengo, P. Salati, Phys. Rev. D 62 (2000) 043003, Available from: <hep-ph/9904481>.
[58] G. Servant, T.M.P. Tait, Nucl. Phys. B 650 (2003) 391, Available from: <hep-ph/0206071>.
[59] H.C. Cheng, J.L. Feng, K.T. Matchev, Phys. Rev. Lett. 89 (2002) 211301, Available from: <hep-ph/0207125>.
[60] R.J. Protheroe, Astrophys. J. 254 (1982) 391.
[61] S.W. Barwick et al. [HEAT Collaboration], Phys. Rev. Lett. 75 (1995) 390. Available from: <astro-ph/9505141>.
[62] S.W. Barwick et al. [HEAT Collaboration], Astrophys. J. 482 (1997) L191. Available from: <astro-ph/9703192>.
[63] S. Coutu et al. [HEAT-pbar Collaboration], in: Proceedings of the 27th International Cosmic Ray Conference, 2001.
[64] G.L. Kane, L.T. Wang, J.D. Wells, Phys. Rev. D 65 (2002) 057701, Available from: <hep-ph/0108138>.
[65] E.A. Baltz, J. Edsjo, K. Freese, P. Gondolo, Phys. Rev. D 65 (2002) 063511, Available from: <astro-ph/0109318>.
[66] G.L. Kane, L.T. Wang, T.T. Wang, Phys. Lett. B 536 (2002) 263, Available from: <hep-ph/0202156>.
[67] D. Hooper, J.E. Taylor, J. Silk, Can supersymmetry naturally explain the positron excess? Available from: <hep-ph/0312076>.
[68] F.W. Stecker, Phys. Lett. B 201 (1988) 529.
[69] F.W. Stecker, A.J. Tylka, Astrophys. J. 343 (1989) 169.
[70] L. Bergström, P. Ullio, J.H. Buckley, Astropart. Phys. 9 (1998) 137, Available from: <astro-ph/9712318>.
[71] V.S. Berezinsky, A.V. Gurevich, K.P. Zybin, Phys. Lett. B 294 (1992) 221.
[72] V. Berezinsky, A. Bottino, G. Mignola, Phys. Lett. B 325 (1994) 136, Available from: <hep-ph/9402215>.
[73] M. Urban, A. Bouquet, B. Degrange, P. Fleury, J. Kaplan, A.L. Melchior, E. Pare, Phys. Lett. B 293 (1992) 149, Available from: <hep-ph/9208255>.
[74] P. Gondolo, J. Silk, Phys. Rev. Lett. 83 (1999) 1719, Available from: <astro-ph/9906391>.
[75] L. Bergström, J. Edsjö, P. Ullio, Phys. Rev. D 58 (1998) 083507, Available from: <astro-ph/9804050>.
[76] L. Bergström, J. Edsjö, P. Gondolo, P. Ullio, Phys. Rev. D 59 (1999) 043506, Available from: <astro-ph/9806072>.
[77] E.A. Baltz, C. Briot, P. Salati, R. Taillet, J. Silk, Phys. Rev. D 61 (2000) 023514, Available from: <astro-ph/9909112>.
[78] S. Rudaz, F.W. Stecker, Astrophys. J. 368 (1991) 406.
[79] L. Bergström, P. Ullio, Nucl. Phys. B 504 (1997) 27, Available from: <hep-ph/9706232>.
[80] Z. Bern, P. Gondolo, M. Perelstein, Phys. Lett. B 411 (1997) 86, Available from: <hep-ph/9706538>.

[81] P. Ullio, L. Bergström, Phys. Rev. D 57 (1998) 1962, Available from: <hep-ph/9707333>.
[82] V.S. Berezinsky, A. Bottino, V. de Alfaro, Phys. Lett. B 274 (1992) 122.
[83] K. Freese, Phys. Lett. B 167 (1986) 295.
[84] L.M. Krauss, M. Srednicki, F. Wilczek, Phys. Rev. D 33 (1986) 2079.
[85] T.K. Gaisser, G. Steigman, S. Tilav, Phys. Rev. D 34 (1986) 2206.
[86] A. Gould, J.A. Frieman, K. Freese, Phys. Rev. D 39 (1989) 1029.
[87] A. Bottino, N. Fornengo, G. Mignola, L. Moscoso, Astropart. Phys. 3 (1995) 65, Available from: <hep-ph/9408391>.
[88] V. Berezinsky, A. Bottino, J.R. Ellis, N. Fornengo, G. Mignola, S. Scopel, Astropart. Phys. 5 (1996) 333, Available from: <hep-ph/9603342>.
[89] W.H. Press, D.N. Spergel, Astrophys. J. 296 (1985) 679.
[90] J. Silk, K. Olive, M. Srednicki, Phys. Rev. Lett. 55 (1985) 257.
[91] M. Srednicki, K.A. Olive, J. Silk, Nucl. Phys. B 279 (1987) 804.
[92] J.S. Hagelin, K.W. Ng, K.A. Olive, Phys. Lett. B 180 (1986) 375.
[93] K. Ng, K.A. Olive, M. Srednicki, Phys. Lett. B 188 (1987) 138.
[94] J. Ellis, R.A. Flores, Nucl. Phys. B 307 (1988) 883.
[95] J.L. Feng, K.T. Matchev, F. Wilczek, Phys. Rev. D 63 (2001) 045024, Available from: <astro-ph/0008115>.
[96] J.D. Lykken, K.T. Matchev, Phys. Rev. D 61 (2000) 015001, Available from: <hep-ph/9903238>; Tau jet signals for supersymmetry at the Tevatron. Available from: <hep-ex/9910033>.
[97] K.T. Matchev, D.M. Pierce, Phys. Rev. D 60 (1999) 075004, Available from: <hep-ph/9904282>.
[98] K.T. Matchev, D.M. Pierce, Phys. Lett. B 467 (1999) 225, Available from: <hep-ph/9907505>.
[99] G.F. Giudice, R. Rattazzi, Phys. Rept. 322 (1999) 419, Available from: <hep-ph/9801271>.
[100] H. Pagels, J.R. Primack, Phys. Rev. Lett. 48 (1982) 223.
[101] S. Weinberg, Phys. Rev. Lett. 48 (1982) 1303.
[102] L.M. Krauss, Nucl. Phys. B 227 (1983) 556.
[103] D.V. Nanopoulos, K.A. Olive, M. Srednicki, Phys. Lett. B 127 (1983) 30.
[104] M.Y. Khlopov, A.D. Linde, Phys. Lett. B 138 (1984) 265.
[105] J.R. Ellis, J.E. Kim, D.V. Nanopoulos, Phys. Lett. B 145 (1984) 181.
[106] R. Juszkiewicz, J. Silk, A. Stebbins, Phys. Lett. B 158 (1985) 463.
[107] M. Bolz, A. Brandenburg, W. Buchmuller, Nucl. Phys. B 606 (2001) 518, Available from: <hep-ph/0012052>.
[108] J.L. Feng, A. Rajaraman, F. Takayama, Phys. Rev. Lett. 91 (2003) 011302, Available from: <hep-ph/0302215>.
[109] J.L. Feng, A. Rajaraman, F. Takayama, Phys. Rev. D 68 (2003) 063504, Available from: <hep-ph/0306024>.
[110] L. Covi, J.E. Kim, L. Roszkowski, Phys. Rev. Lett. 82 (1999) 4180, Available from: <hep-ph/9905212>.
[111] L. Covi, H.B. Kim, J.E. Kim, L. Roszkowski, JHEP 0105 (2001) 033, Available from: <hep-ph/0101009>.
[112] L. Covi, L. Roszkowski, R. Ruiz de Austri, M. Small, Axino dark matter and the CMSSM. Available from: <hep-ph/0402240>.
[113] D. Hooper, L.T. Wang, Evidence for axino dark matter in the galactic bulge. Available from: <hep-ph/0402220>.
[114] J.L. Feng, A. Rajaraman, F. Takayama, Phys. Rev. D 68 (2003) 085018, Available from: <hep-ph/0307375>.
[115] J. Ellis, K.A. Olive, Y. Santoso, V.C. Spanos, Gravitino dark matter in the CMSSM. Available from: <hep-ph/0312262>.
[116] J. Ellis, K.A. Olive, Y. Santoso, V.C. Spanos, Very constrained minimal supersymmetric standard models. Available from: <hep-ph/0405110>.
[117] J.L. Feng, T. Moroi, Phys. Rev. D 58 (1998) 035001, Available from: <hep-ph/9712499>.
[118] D. Acosta, Talk given at the 14th Topical Conference on Hadron Collider Physics, September 29–October 4, 2002, Germany.

[119] X. Chen, M. Kamionkowski, Particle decays during the cosmic dark ages. Available from: <astro-ph/0310473>.
[120] K. Sigurdson, M. Kamionkowski, Charged-particle decay and suppression of small-scale power. Available from: <astro-ph/0311486>.
[121] J.R. Ellis, D.V. Nanopoulos, S. Sarkar, Nucl. Phys. B 259 (1985) 175.
[122] J.R. Ellis, G.B. Gelmini, J.L. Lopez, D.V. Nanopoulos, S. Sarkar, Nucl. Phys. B 373 (1992) 399.
[123] M. Kawasaki, T. Moroi, Astrophys. J. 452 (1995) 506, Available from: <astro-ph/9412055>.
[124] E. Holtmann, M. Kawasaki, K. Kohri, T. Moroi, Phys. Rev. D 60 (1999) 023506, Available from: <hep-ph/9805405>.
[125] M. Kawasaki, K. Kohri, T. Moroi, Phys. Rev. D 63 (2001) 103502, Available from: <hep-ph/0012279>.
[126] T. Asaka, J. Hashiba, M. Kawasaki, T. Yanagida, Phys. Rev. D 58 (1998) 023507, Available from: <hep-ph/9802271>.
[127] R.H. Cyburt, J. Ellis, B.D. Fields, K.A. Olive, Phys. Rev. D 67 (2003) 103521, Available from: <astro-ph/0211258>.
[128] M.H. Reno, D. Seckel, Phys. Rev. D 37 (1988) 3441.
[129] S. Dimopoulos, R. Esmailzadeh, L.J. Hall, G.D. Starkman, Nucl. Phys. B 311 (1989) 699.
[130] M.Y. Khlopov, Cosmoparticle Physics, World Scientific, Singapore, 1999.
[131] K. Kohri, Phys. Rev. D 64 (2001) 043515, Available from: <astro-ph/0103411>.
[132] K. Hagiwara et al. [Particle Data Group Collaboration], Phys. Rev. D 66 (2002) 010001.
[133] R.H. Cyburt, B.D. Fields, K.A. Olive, Phys. Lett. B 567 (2003) 227, Available from: <astro-ph/0302431>.
[134] D. Kirkman, D. Tytler, N. Suzuki, J.M. O'Meara, D. Lubin, Astrophys. J. Suppl. 149 (2003) 1, Available from: <astro-ph/0302006>.
[135] S. Burles, K.M. Nollett, M.S. Turner, Astrophys. J. 552 (2001) L1, Available from: <astro-ph/0010171>.
[136] K. Jedamzik, Phys. Rev. Lett. 84 (2000) 3248, Available from: <astro-ph/9909445>.
[137] K. Jedamzik, Did something decay, evaporate, or annihilate during big bang nucleosynthesis. Available from: <astro-ph/0402344>.
[138] M. Kawasaki, K. Kohri, T. Moroi, Hadronic decay of late-decaying particles and big-bang nucleosynthesis. Available from: <astro-ph/0402490>.
[139] J.L. Feng, S.f. Su, F. Takayama, SuperWIMP gravitino dark matter from slepton and sneutrino decays. Available from: <hep-ph/0404198>.
[140] J.L. Feng, S. Su, F. Takayama, Supergravity with a gravitino LSP. Available from: <hep-ph/0404231>.
[141] W. Buchmuller, K. Hamaguchi, M. Ratz, T. Yanagida, Phys. Lett. B 588 (2004) 90, Available from: <hep-ph/0402179>.
[142] W. Buchmuller, K. Hamaguchi, M. Ratz, T. Yanagida, Gravitino and goldstino at colliders. Available from: <hep-ph/0403203>.
[143] F. Wang, J.M. Yang, SuperWIMP dark matter scenario in light of WMAP. Available from: <hep-ph/0405186>.
[144] W. Hu, J. Silk, Phys. Rev. Lett. 70 (1993) 2661.
[145] D.J. Fixsen, et al., Astrophys. J. 473 (1996) 576, Available from: <astro-ph/9605054>.
[146] Available from: <http://map.gsfc.nasa.gov/DIMES>.
[147] J.L. Feng, M.M. Nojiri, Supersymmetry and the linear collider. Available from: <hep-ph/0210390>.
[148] Available from: <http://www.rssd.esa.int/index.php?project=PLANCK>.
[149] M. Drees, Y.G. Kim, M.M. Nojiri, D. Toya, K. Hasuko, T. Kobayashi, Phys. Rev. D 63 (2001) 035008, Available from: <hep-ph/0007202>.
[150] J.L. Feng, M.E. Peskin, H. Murayama, X. Tata, Phys. Rev. D 52 (1995) 1418, Available from: <hep-ph/9502260>.
[151] R.D. Peccei, H.R. Quinn, Phys. Rev. D 16 (1977) 1791.
[152] S. Weinberg, Phys. Rev. Lett. 40 (1978) 223.
[153] F. Wilczek, Phys. Rev. Lett. 40 (1978) 279.

[154] A. Kusenko, M.E. Shaposhnikov, Phys. Lett. B 418 (1998) 46, Available from: <hep-ph/9709492>.
[155] A. Kusenko, V. Kuzmin, M.E. Shaposhnikov, P.G. Tinyakov, Phys. Rev. Lett. 80 (1998) 3185, Available from: <hep-ph/9712212>.
[156] K. Enqvist, A. Mazumdar, Phys. Rept. 380 (2003) 99, Available from: <hep-ph/0209244>.